Quantum Molecular Dynamics on Grids

Ronnie Kosloff

Department of Physical Chemistry and the Fritz Haber Research Center,

the Hebrew University, Jerusalem 91904, Israel

Contents

I. INTRODUCTION

Molecular dynamics is the study of basic principles of chemical change. It's underlying theory is either classical or quantum mechanics. Much of the original insight into molecular encounters stemmed from a classical picture where the atoms were imagined to be positioned in three dimensional coordinate space. This picture is in conflict with the quantum mechanical viewpoint that particles do not possess a definite position. A true quantum image of the particle is now understood as a blurred object able to interfere with itself.

The traditional development of quantum mechanics has been heavily influenced by the work of Hilbert, describing the wavefunction Ψ by a functional expansion $\Psi = \sum_n a_n \phi_n$. This formulation created a powerful theory which has been translated in to an effective computational scheme based on linear algebraic methods. These algebraic methods have become the main agents of quantum molecular dynamical computations, but have blurred the image of the molecular encounter. The algebraic approach has created a new language in which, for example, a chemical reaction is described by a matrix quantity, the state-to-state

transition amplitude S_{ij}.

The lack of a clear image in quantum molecular dynamics has been a handicap for most researchers. This is in comparison to classical molecular dynamics which is strongly linked to the notion of a trajectory, a causal path leading from reactants to products. Imaging the flow of a trajectory constitutes one of the main sources of insight on classical molecular dynamics.

The historical development of quantum molecular dynamics abandoned the causal framework based on time-dependent formalism and adopted a time-independent framework. This was despite the fact that causal interpretation of events, where a cause in the past leads to a result in the future is strongly imprinted in human thought. In the time independent formalism the stationary currents become the source of imagery, a tool which has rarely been used. As a result, molecular dynamics has had to face the problem that intuitive insight has been heavily based on classical mechanics, while quantitative predictions have been based on quantum dynamics.

One way out of the discrepancy has been to augment the classical description with quantum corrections. This has been the motivation for the large effort put into developing semiclassical methods in molecular dynamics [1–5]. Such a line of thought has not been followed in this chapter which follows a bolder approach based on quantum methods in the time-domain where the wavefunction is represented directly in configuration space. Two questions are raised by this endeavor:

a) Can new insight on molecular encounters be gained from a quantum coordinate representation in the time domain?

b) Can an efficient and accurate computational method be developed based on these representations?

The purpose of this chapter is to show that these two questions can be answered positively based on a grid description and computation scheme.

The historical development of grid methods in molecular dynamics can be traced to the early work of McCullough and Wyatt [6,7] who used a direct finite differencing (FD) scheme

to solve the collinear H + H_2 reactive scattering problem. Their work then utilized two important imaging tools: snapshots of contour plots of the absolute value of the wavefunction and flux maps. Numerical improvement of the original method was introduced by Askar [8] who suggested a replacement of the Crank-Nicholson propagator by the second order differencing scheme (SOD). At the time, the numerical accuracy and efficiency of the FD method was not sufficient to compete with the time-independent spectral quantum methods for reactive scattering. As a result, the FD methods were almost abandoned. (As an exception FD methods became popular in the calculations of above threshold ionization ATI due to their ability to tolerate the coulomb singularity without contaminating the rest of the wavefunction. [9]) In section III an analysis of why finite difference methods are hard to converge will be presented.

It was the introduction of the Fourier based pseudo-spectral methods [10–12] which created a grid based method with high accuracy and efficiency. This development was supplemented by the more general pseudo-spectral methods introduced into molecular dynamics by Light, Hamilton, and Lill [13] which greatly increased the applicability of grid based methods. Another important development was the Chebychev based propagator [14] which became the base for the development of spectral and pseudo-spectral methods in the time-energy phase space. Recent developments in implementing propagator techniques have made the distinction between time-dependent and time-independent methods almost vanish [15]. Currently, due to the efforts of many people, time-dependent and time-independent grid based methods are able to create imagery as well as high quality, first principle simulations, of molecular encounters.

II. GENERAL SETUP OF GRID METHODS

When simulating a molecular encounter experiment, it is wise to define the framework of the simulation before attempting to perform it. The duration of the experiment will be limited by the patience of the experimentalist of course , but more precisely a typical

molecular encounter is completed in a few femtoseconds up to a few picoseconds. The next task in setting the simulation is to count the number of particles or the number of degrees of freedom in the problem. Each particle is to be contained in a finite volume which for a typical encounter is between 10 to 1000 Å^3. Finally, the energy range of a molecular encounter ΔE is to be set, typically in the range of 0-10 eV. Once this arena of the simulation has been worked out, its computational feasibility can be determined.

The next step is to realize that the arena of molecular change is the phase space $\{p, q\}$, which is true for both classical and quantum mechanics. The "volume" of the position-momentum phase space containing the encounter can be estimated from the range of position and momentum. The maximum momentum can be determined from the energy range $|P_{max}| < \sqrt{2mE_{max}}$. This estimate has to be repeated for each degree of freedom. The range of position is also determined by a condition on the potential $V(q_{max}) < E_{max}$. The molecular encounter takes place in a volume that is a direct product of the position momentum phase space $\{p, q\}$ of all degrees of freedom and of the time-energy phase space $\{t, E\}$.

Figure 2.1 shows the volume containing the molecular encounter and its projections on the $\{q, p\}$ phase space and the $\{t, E\}$ phase space. In classical mechanics, the encounter is described by a thread running through the volume $\{q, p\} \otimes \{t, E\}$. In quantum mechanics, a global description of this "volume" is required. From quantum statistical mechanics it can be concluded that a sufficient sampling is obtained if this "volume" is divided by h for each spatial and time dimension. This leads to the number of grid points necessary for sufficient sampling $N_g \approx \mathcal{V}/h^N$ for N spatial dimensions, and $N_t \approx \Delta E \cdot T/\hbar$ (see figure 2.1).

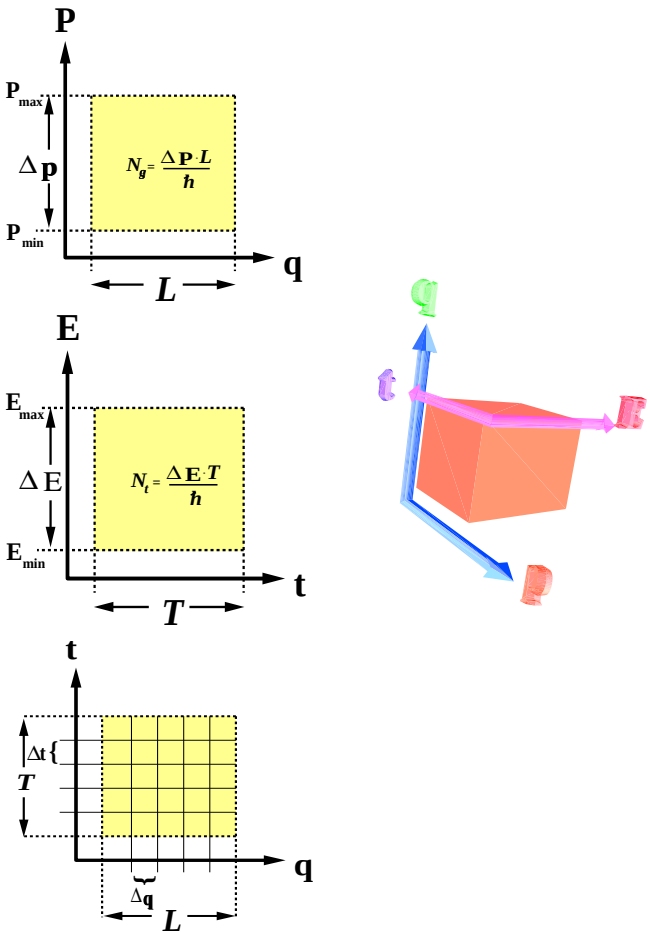

FIGURE 2.1 A schematic description of the arena of a molecular encounter. The "volume" on the right represents a 3-dimensional projection of the four-dimensional phase space volume $\mathcal{V} = \{q, p\} \otimes \{t, E\}$. Each degree of freedom can be projected onto the three left panels. The lower left panel shows the arena represented directly by the grid.

Representing the wavefunction on a grid can be formally symbolized as: $\Psi(q,t) \rightarrow \Psi(q_i, t_j)$. It will be shown that grid methods are able to to reach a sampling efficiency which is very close to the estimates of h per unit of occupied phase space.

From the estimate of the number of grid points in space, N_g and in time, N_t it can be concluded that any effort that reduces the represented "volume" should be attempted. The influence of "empty volume" increases with the dimensionality of the problem. In one and two dimensional problems one can afford to be sloppy in the representation, but in a high dimensional problem, sloppiness can eliminate the ability to simulate the problem at

all. The way to eliminate empty phase space "volume" is to correlate the representation as much as possible. An extreme example of a correlated state is an energy eigenstate which occupies exactly $\mathcal{V} = h^{N+1}$, or one pixel in hyperspace.

To follow the molecular dynamics means following the evolution of the wavefunction through time $\Psi(q, t+T) = \mathbf{U}(T)\Psi(q,t)$. In the discrete representation this evolution is manifested as a discrete mapping of the wavefunction $\Psi(q_i, t_j)$ into the same discrete space: $\Psi(q_j, t_l + T)$. This goal will be obtained in two stages: the first is the study of the discrete mapping produced by the Hamiltonian operator: $\Phi = \mathbf{H}\Psi$ i.e. obtaining $\Phi(q_j)$ from $\Psi(q_i)$. The second stage is implementing the evolution operator based on this mapping. The development of these steps will be described in sections III and section V.

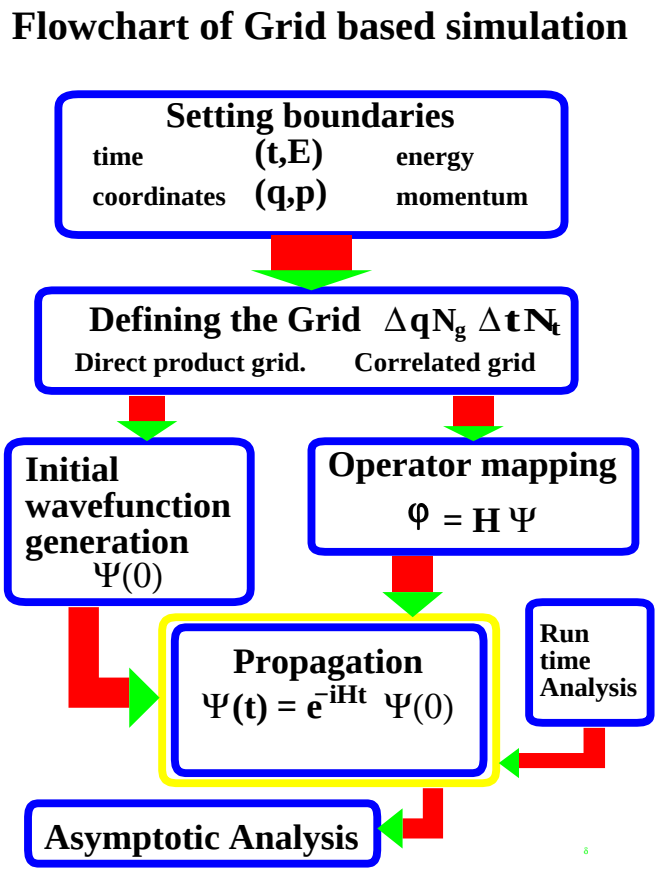

FIGURE 2.2 The flowchart of the generic simulation of a molecular dynamical event based on grid schemes.

III. REPRESENTATION OF THE WAVEFUNCTION Ψ ON A SPATIAL GRID

The discrete representation of the wavefunction can be imagined as viewing the world through a set of port-holes. Since we know that the viewed wavefunction is continuous, by interpolating between the individual pictures the global landscape can be reconstructed. This concept, which forms the basis of representation theory, enables the reconstruction of the full position-momentum phase space.

There are two approaches to such interpolation, a local and a global one. The local approach is based on a set of piecewise-continuous functions, usually polynomials. These functions are designed to interpolate locally between the grid points. The interpolation process allows the derivatives on the points to be defined since it is based on analytically continuous functions. This local interpolation is the basis of the finite difference method (FD).

The global approach uses an interpolation based on a family of global functions which span all the sampled space with appropriate boundary conditions. This approach which is due to Gauss, is termed collocation (Subsection III A). In a more elaborate form, based on orthogonal functions it is termed *pseudo-spectral representation* (subsection III B) [16]. Since any local method is global within a small interval we will start by analysing global approaches.

A global approximation of a wavefunction $\psi(q)$ by a finite set of N_f functions $g_n(q)$ becomes

$$\psi(q) \approx \bar{\psi}(q) = \sum_{n=0}^{N_f-1} a_n \, g_n(q) \, , \tag{3.1}$$

where $g_n(q)$ are analytic functions in the domain of interest, obeying the appropriate boundary conditions. The finite representation problem is recast as a method of obtaining the expansion coefficients a_n once the functions $g_n(q)$ are known.

A. General Collocation Method

In mathematical terms, the collocation method determines the expansion coefficients by matching the approximate solution to the true solution on a set of $N_g = N_f$ grid points,

$$\psi(q_j) \equiv \bar{\psi}(q_j) = \sum_{n=0}^{N_g-1} a_n \, g_n(q_j) \, , \tag{3.2}$$

where the q_j are the collocation points. These are the sampling points shown in figure 3.1 .

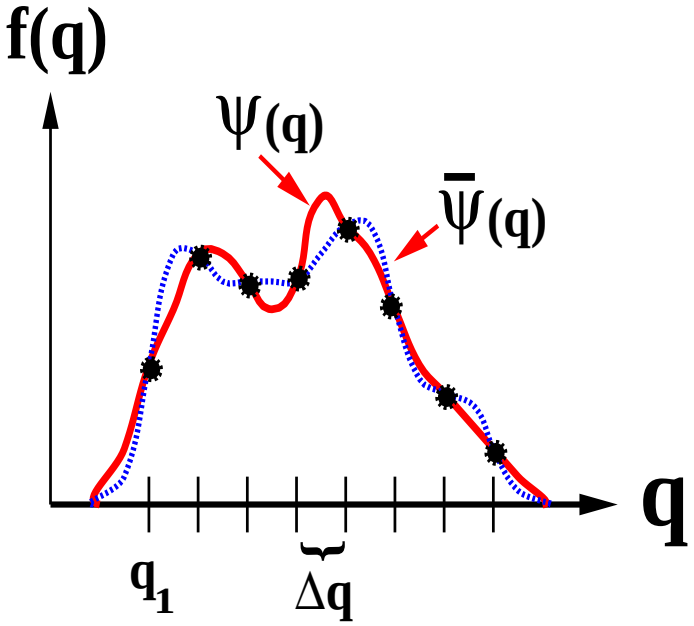

FIGURE 3.1 An interpolation of the wavefunction ψ (solid) by its approximation $\bar{\psi}$(dashed). The approximate and the original functions are identical on the sampling points q_i.

Equation (3.2) is equivalent to a set of coupled linear equations. In matrix form they become

$$\psi = \mathbf{G}\,\mathbf{a} \, , \tag{3.3}$$

where $\psi_j = \psi(q_j)$ and the matrix $G_{nj} = g_n(q_j)$. Provided that the $g_n(q_j)$ are linearly independent, the solution of equation (3.3) becomes:

$$\mathbf{a} = \mathbf{G}^{-1} \, \psi \, . \tag{3.4}$$

The functional basis that supplies the global picture is connected through the expansion coefficients a_n to the spatial grid. This provides the ability to define the scalar product of two functions. If

$$\psi(q) \quad = \quad \sum_n \; a_n g_n(q) \tag{3.5}$$

and

$$\phi(q) \quad = \quad \sum_m b_m g_m(q) \tag{3.6}$$

then

$$< \psi | \phi > \; \equiv \; \sum_{nm} S_{nm} a_n{}^* b_m \tag{3.7}$$

where S_{nm} is the overlap matrix

$$S_{nm} \quad = \quad \int_D \; dq \; g_n(q)^* g_m(q) \tag{3.8}$$

and the integration is carried out over the domain D.

Primitive collocation methods, based on general expansion functions g_n, have been developed. An attractive idea has been to distribute localized functions in regions where the wavefunction is expected to have a high probability. Such a method, using a set of distributed Gaussian functions, has been developed by Hamilton and Light [17]. Attempts to use wavelets as a localized base have also been reported. Nevertheless the numerical experience with these methods has not been satisfactory. The main drawback of primitive collocation schemes is over-completeness of the representation which leads to a reduction in the rank of the overlap matrix S. This problem causes numerical singularities in the inversion of the **G** matrix. Such a phenomenon can also be understood from the perspective of Gram-Schmidt orthogonalization. Functions which have nearly complete overlap will cause extreme numerical sensitivity upon orthogonalization.

This problem can be overcome by the use of orthogonal expansion functions. (The subject of the next subsection). Another possible numerical fix is to use more sampling points than functions. The over determination of the inversion is overcome by a least squares procedure [18].

B. Orthogonal Collocation Schemes

A great simplification in the collocation scheme is achieved if the set of expansion functions $g_n(q)$ obey the orthogonality relation

$$\sum_{n=0}^{N_g-1} g_n(q_i) g_n^*(q_j) \;=\; \delta_{ij} \;, \tag{3.9}$$

allowing a direct inversion for the expansion coefficients a_n in equation (3.3):

$$a_n \;=\; \sum_{j=0}^{N_g-1} \psi(q_j) g_n^*(q_j) \;. \tag{3.10}$$

This means that the expansion coefficients a_n are the discrete functional transform of the function ψ. On the other hand, if

$$< g_n | g_m > \;=\; \int_D dq \; g_n(q) g_m^*(q) \;=\; \delta_{nm} \quad , \tag{3.11}$$

then the scalar product in equation (3.7) is greatly simplified leading to:

$$< \psi | \phi > \;=\; \sum_n \; {a_n}^* b_n \tag{3.12}$$

which, using equation (3.9), becomes:

$$< \psi | \phi > \;=\; \sum_{j=0}^{N_g-1} \; \psi^*(q_j) \phi(q_j) \;. \tag{3.13}$$

A consequence of the orthogonality relations is that the collocation functional expansion scheme becomes a discrete vector space with a unitary transformation between the discrete sampling points q_j and the discrete functional base a_n. The matrix $\mathbf{G}$ is then unitary.

At this point, it is appropriate to compare the collocation method with the traditional variation approach to the functional expansion problem. The variational approach minimizes the functional:

$$\mathcal{J} \;=\; \int_D d\mathbf{q} \; |\psi(q) - \bar{\psi}(q)|^2 \;. \tag{3.14}$$

Here, $\mathcal{J}$ is the averaged squared difference between the function ψ and its approximation $\bar{\psi}$, and D is the domain of interest, leading to the determination of a_n by the relation $\delta \mathcal{J} \;=\; 0$.

If the expansion functions are orthogonal, $< g_n|g_m >= \delta_{nm}$, then the expansion coefficients become the functional transform of ψ:

$$\bar{a}_n \;\; = < \psi|g_n > \;\; = \;\; \int_D dq\psi(q)g_n^*(q) \tag{3.15}$$

This method will be referred to as the variational spectral method [19]. At this point one can approximate the integral in Eq. (3.15) by a Gaussian quadrature of N points:

$$\bar{a}_n \;\; \approx \;\; \sum_{l=0}^{N-1} \; \psi(q_l){g_n}^*(q_l)W(q_l) \qquad . \tag{3.16}$$

Based on the Christoffel-Darboux formula [20] it can be shown that this procedure leads to a functional expansion which becomes an interpolation formula on the integration points, $\bar{\psi}(q_k) \equiv \psi(q_k)$. As an example consider an expansion by the Chebychev orthogonal polynomials $g_n(q) = T_n(q)$ with the constant weights $W(q_l) = \frac{2}{\pi}$. The quadrature points q_l are the zeros of the Chebychev polynomial of degree $N+1$. On inserting equation (3.16) into the functional expansion Eq. (3.2) becomes:

$$\begin{aligned} \sum_{n=0}^{N-1} \; \bar{a}_n T_n(q_k) \;\; &= \;\; \frac{2}{\pi} \sum_{n=0}^{N-1} \sum_{l=0}^{N-1} \; \psi(q_l)T_n(q_l)T_n(q_k) \\ = \;\; \sum_{l=0}^{N-1} \; \psi(q_l) \; \frac{2}{\pi} \sum_{n=0}^{N-1} \; T_n(q_l)T_n(q_k) \;\; &= \;\; \psi(q_k) \end{aligned} \tag{3.17}$$

and therefore $\bar{\psi}(q_k) \equiv \psi(q_k)$. The last equation is because of changing the order of summation and the Christoffel-Darboux formula [20], which for the Chebychev polynomials reads: $2/\pi \sum_{n=0}^{N-1} \; T_n(q_l)T_n(q_k) \;\; = \;\; \delta_{lk}$. From equation (3.17), it can be concluded that the Chebychev variational expansion is equivalent to a polynomial interpolation when the sampling points are the zeros of the $N+1$ Chebychev polynomial and the expansion coefficients are calculated using the Gauss-Chebychev quadrature scheme of order N (See also subsection III E). In general this means that the variational and the collocation methods based on orthogonal expansion functions are closely related and therefore their quality of representation is numerically equivalent.

Section III D will elaborate on a particular choice of orthogonal functions, the Fourier set.

C. Direct grid collocation methods

A direct inversion of the collocation representation Eq. (3.1) where the expansion coefficients a_n become the values of the function at the interpolation points $a_n = \psi(q_n)$ can be obtained with a proper choice of expansion functions $g_n(q)$. This representation is generated by a global function $U_{N_g}(q)$ which has N_g simple zeros at the interpolation points: $U_{N_g}(q_j) = 0$ for all grid points j. Then

$$\bar{\psi}(q) \quad = \quad \sum_{j=0}^{N_g-1} \psi(q_j) \frac{U_{N_g}(q)}{(q-q_j) U_{N_g}{}'(q_j)} \tag{3.18}$$

is an interpolation formula [21], where $U_{N_g}{}'(q_j)$ is the derivative of $U_{N_g}(q)$ at the interpolation point q_j. The structure of the expansion functions: $g_n(q) = \frac{U_{N_g}(q)}{(q-q_j)U_{N_g}{}'(q_n)}$, is responsible for the direct inversion property. The value of the function is one on grid point q_n and zero on all other grid points (see figure 3.2)

Choosing the generating function U_{N_g} as the polynomial,
$U_{N_g}(q) = (q-q_1)(q-q_2)...(q-q_j)...(q-q_{N_g})$ leads to the well known Lagrange interpolation formula. Figure III C shows the expansion function $g_n(q)$ which is based on the zeros of the Chebychev orthogonal polynomial of order N_g.

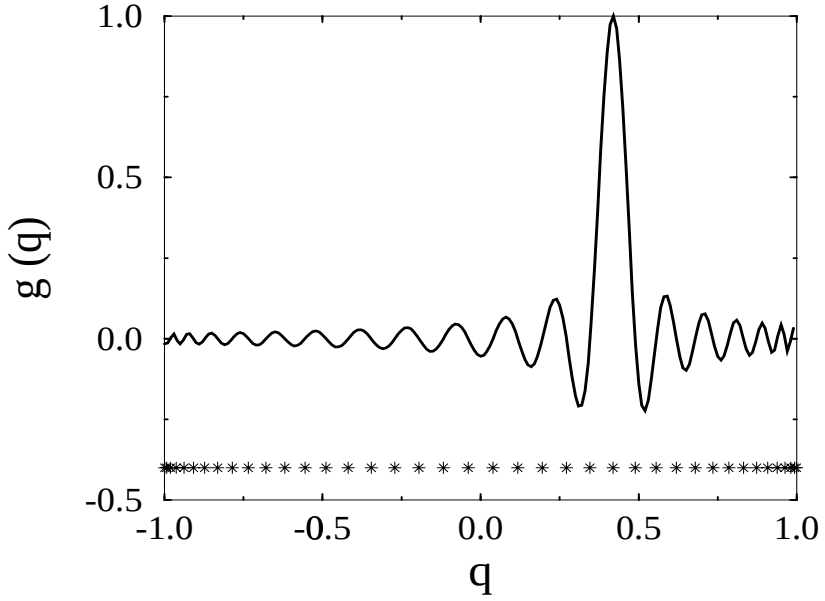

FIGURE 3.2 The direct grid interpolation function $g_n(q)$, ($n = 15$, $N_g = 40$) for Chebychev

interpolation points. The function $g_n(q)$ equals one on grid point $n = 15$, and zero at all other grid points. The 40 interpolation points are shown as stars at the bottom of the plot.

Another choice appropriate for evenly distributed sampling points is based on the global function $U_{N_g}(q) = \sin(2\pi q/\Delta q)$. It is closely related to the Fourier method described in the next section.

D. The Fourier Method

An examination of the Fourier method, which is a special case of an orthogonal collocation representation, elucidates the main considerations of representation theory. It will be shown that by optimizing the representation the quantum limit of one point per unit phase space volume of h can be obtained. Moreover, the Fourier method has great numerical advantages because of the "fast" nature of the algorithm [22–26]. This means that the numerical effort scales semi-linearly with the represented volume of phase space [27].

In the Fourier method, the orthogonal functions $g_n(q)$ are chosen as [12,28,27]

$$g_k(q) \;=\; e^{i2\pi kq/L} \quad , \quad k \;=\; -(N_g/2-1), ..., 0, ..., N_g/2 \tag{3.19}$$

leading to N_g equally spaced sampling points where $q_j \;=\; (j-1)\Delta q$, $(j = 1, ...N_g)$ and L is the length of the interval. Using the relation $L \;=\; N_g\Delta q$, the completeness relations of the Fourier expansion functions become

$$\sum_{k=-N_g/2-1}^{N_g/2} g_k(q_n)g_k^*(q_m) \;=\; \sum_{k=-(N_g/2-1)}^{N_g/2} e^{i2\pi kq_n/L}e^{-i2\pi kq_m/L} \;=$$

$$\sum_{k=-(N_g/2-1)}^{N_g/2-1} e^{i2\pi kn/N_g}e^{-i2\pi km/N_g} \;=\; e^{-i2\pi(n-m)/N_g}\frac{1-e^{i2\pi(n-m)}}{1-e^{i2\pi(n-m)/N_g}} \;=\; \delta_{nm}N_g \tag{3.20}$$

where the summation can be carried out explicitly because it is a geometric series. The fourth equality in equation (3.20) follows because if $n = m$ the summation is trivial. Otherwise, $|n-m|$ ranges from 1 to N_g-1 and is never an integral multiple of N_g. Thus the denominator

never vanishes while the numerator is identically zero. This is the first orthogonality relation, equation (3.9).

The second orthogonality relation equivalent to equation (3.11) becomes

$$\frac{1}{2\pi}\int_{-\pi}^{\pi} e^{imq'}e^{-inq'}dq' \;=\; \frac{1}{2\pi}\left[\;\frac{1}{i(m-n)}\;e^{i(m-n)q}\;\right]_{-\pi}^{\pi} \;=\; \delta_{nm} \tag{3.21}$$

where $q' \;=\; \pi(q/L \;-\; 1)$, $0 \leq q \leq L$. These relationships imply that the domain D has periodic boundary conditions. The symmetry between n and k in equation (3.20) leads to the discrete version of equation (3.21):

$$\sum_{j=1}^{N_g} g_k(q_j)g_l^*(q_j) \;=\; \delta_{kl}N_g \qquad |k-j| < N_g\ . \tag{3.22}$$

The Fourier expansion of a wavefunction $\psi(q)$ is next explored:

$$\psi(q) \;\approx \sum_{k=-(N_g/2-1)}^{N_g/2} a_k e^{i2\pi kq/L}\ . \tag{3.23}$$

The expansion coefficients a_k become the discrete Fourier expansion coefficients. The orthogonality of the Fourier functions with equidistant sampling points can be used to invert the relation giving:

$$a_k \;=\; \frac{1}{N}\sum_{j=1}^{N_g} \psi(q_j)e^{-i2\pi kq_j/L}\ . \tag{3.24}$$

Thus, the adjoint relationship, expressed by the matrix $\mathbf{G}$, is particularly simple. In quantum mechanics the coefficients a_k have an important interpretation since they represent the amplitude of the wavefunction in momentum space. Equation (3.23) and equation (3.24) are direct analogues to the continuous Fourier transformation, which changes a coordinate representation to a momentum representation:

$$\begin{cases} \psi(q) \;=\; \frac{1}{\sqrt{2\pi}}\int_{-\infty}^{\infty} e^{\,ikq}\tilde{\psi}(k)dk \\ \tilde{\psi}(k) \;=\; \frac{1}{\sqrt{2\pi}}\int_{-\infty}^{\infty} e^{-ikq}\psi(q)dq \end{cases} \tag{3.25}$$

This means that the expansion coefficient a_k can be interpreted as the value of the wavefunction in the momentum representation at the discrete point k: $a_k = \bar{\psi}(p_k)$, and a momentum evenly spaced grid is automatically constructed with the grid spacing $\Delta p = 2\pi/L$.

The phase space representation of the Fourier method is of a rectangular shape. The volume in phase space covered by the Fourier representation is calculated as follows: The length of the spatial dimension in phase space is $\mathbf{L}$, and the maximum momentum is $\mathbf{p_{max}}$. Therefore, the represented volume becomes $\mathcal{V} = 2\mathbf{L} \cdot \mathbf{p_{max}}$, where the factor of two appears because the momentum range is from $-\mathbf{p_{max}}$ to $+\mathbf{p_{max}}$. Using the fact that $\mathbf{p} = \hbar\mathbf{k}$, the phase space volume can be expressed as

$$\mathcal{V} = 2\hbar\, \mathbf{L} \cdot \mathbf{k_{max}} = N_g h \,, \tag{3.26}$$

where N_g is the number of sampling points. Equation 3.26 is the desired link between the sampled phase space volume and the number of grid points N_g. Since $L = N\Delta q$, it follows that the sampling spacing Δq is related to the maximum wave vector via

$$\Delta q = \frac{\pi}{|\mathbf{k_{max}}|} \,. \tag{3.27}$$

The computational scaling properties of the Fourier method are a result of the scaling properties of the FFT algorithm which scales as $O(N_g \log N_g)$. As a result the phase space volume determines the scaling of the computational effort: $O(\mathcal{V} \log \mathcal{V})$.

A function that is compact in momentum space is equivalent to the band limited Fourier transform of the function. Confinement of such a function to a finite volume in phase space is equivalent to a band limited function with finite support. (The support of a function is the set for which the function is nonzero). The accuracy of a representation of this function is assured by the Whittaker-Kotel'nikov-Shannon sampling theorem [29–31]. It states that a band limited function with finite support is fully specified, if the functional values are given by a discrete, sufficiently dense set of equally spaced sampling points. The number of points is determined by equation (3.26). This implies that a value of the function at an intermediate point can be interpolated with any desired accuracy. This theorem also implies a faithful representation of the n'th derivative of the function inside the interval of support. In other words, a finite set of well-chosen points yields arbitrary accuracy.

Since the wavefunctions are band limited Eq. (3.23) equals the sum of *sinc* functions: $\psi(q) = \sum_{n=-(N_g/2-1)}^{N_g/2} \psi(n\Delta q) sinc[k_{max}(q - n\Delta q)]$. The relation is a consequence of the fact that the *sinc* function is the Fourier transform of a band (rectangel). See also Eq. (3.18).

For unbounded problems, such as occur in quantum mechanics, the wavefunction cannot be confined in both co-ordinate and momentum space. In principle, no wavefunction is strictly band limited with finite support. The idea of a wavepacket, a wavefunction that is almost band limited, is central to the use of the discrete representation.

A wavepacket is a wavefunction that is semi-localized in phase space.

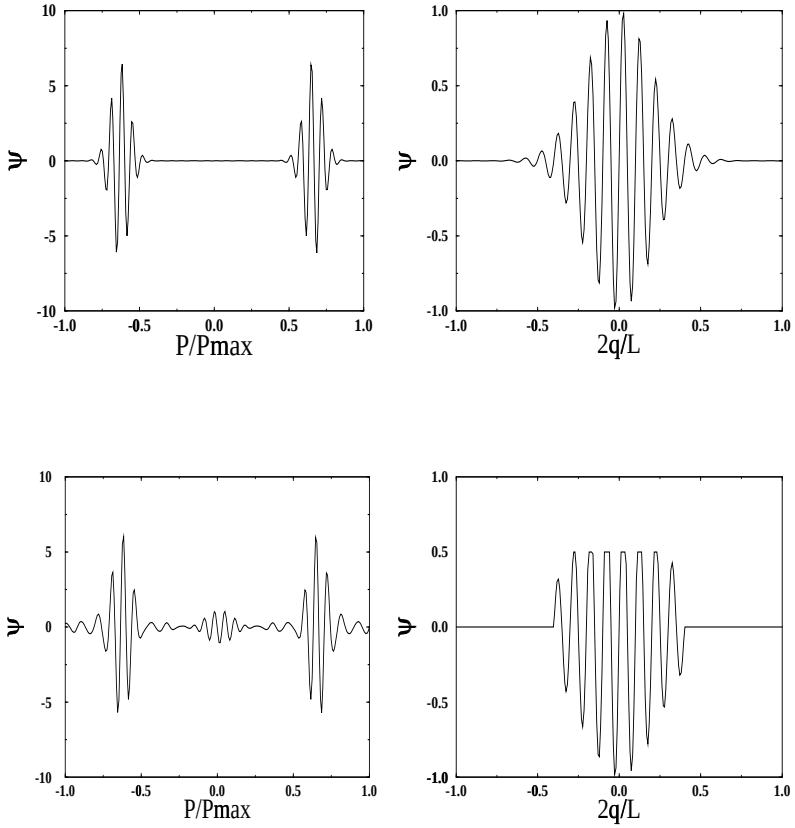

FIGURE 3.3 Upper panel: A wavepacket, a semi-localized wavefunction in coordinate space (right panel) and in momentum space (left panel). (where: $P_{max} = \pi/\Delta q$, L is the interval length: $L = N_g \Delta q$). For the wavepacket the convergence of the expansion (3.23) with respect to N_g is exponential: $O(e^{-\alpha N_g})$. Lower panel: A localized wavefunction in coordinate space but due to the sharp cutoff it is not localized in

momentum space (left lower panel). Convergence with respect to N_g is only $O(1/N_g)$.

The most well-studied example of a wavepacket is the Gaussian wavefunction [1]. Although its wavefunction is not confined to a finite volume, the amplitude outside this volume in phase space converges exponentially to zero in either coordinate or momentum space. This exponential convergence is typical of a good representation of phase space. A counter-example is supplied by a rectangular packet. In coordinate space the wavefunction is well-confined, but in momentum space the rectangular wavefunction is transformed to $\bar{\psi}(k) = A\frac{\sin(a(k-k_0))}{a(k-k_0)}$, which has only a linear convergence rate with the size of the grid in $\mathbf{k}$ space (see figure 3.3). This point is central to the use of the Fourier method which balances the coordinate and momentum representations. For a time dependent calculation, a phase space box has to be large enough to keep the wavefunction localized at all times or using the above concept conserves the wavepacket property.

E. Collocation by orthogonal polynomials

Orthogonal polynomials are a very useful set of expansion functions on grids. The most simple case is to define $g_n(q)$ as $w(q)P_n(q)$, where $P_n(q)$ is a member of the set of orthogonal polynomials, and $w(q)$ is a weight function. These functions obey the continuous orthogonal relation defined in the domain D:

$$\int_D w(q)P_n^*(q)P_m(q)dq = \delta_{nm} \tag{3.28}$$

If the sampling points q_j are chosen as zeros of the $P_{N_g}(q)$ polynomials: $P_{N_g}(q_j) = 0$, then the theory of Gaussian integration leads to:

$$\sum_{j=0}^{N_g-1} W_j P_n(q_j)P_m(q_j) = \delta_{mn} \tag{3.29}$$

where W_j are point weights. Equation (3.29) is used to invert the collocation relation [32] leading to [33–35]:

$$a_n = \sum_{j=0}^{N_g-1} W_j P_n(q_j)\psi(q_j) \quad . \tag{3.30}$$

The grid points which are the Gauss integration quadrature points can be calculated by diagonalizing the position operator in the collocation basis [36]. Figure 3.2 shows the sampling points of the $P_{40}(q)$ Chebychev polynomial ($P_n(q) = \cos(n\ \cos^{-1}(q))$). The method can be supplemented by including the end points in the grid thus using Gauss Radau or Gauss Labato quadratures [37,38]. The orthogonal polynomials can also be used as a basis for a direct grid representation by choosing $g_j(q) = w_j^{1/2} \sum_{n=0}^{N_g-1} P_n(q_j)P_n(q)$ [39,40].

Part of these ideas are well discussed in the work of Gottlieb and Orszag [19] and are known as the pseudo-spectral method. In molecular dynamics this approach is known as DVR [36].

F. Operators represented by grid methods

Operators in quantum mechanics are determined by their consequences. Operators map the wavefunction ψ into a new state vector:

$$\phi \quad = \quad \mathbf{A}\psi \tag{3.31}$$

This elementary relation has a direct consequence in the discrete representation on the grid:

$$\phi(q_i) \quad = \quad \sum_{j}^{N_g} A_{ij}\psi(q_j) \tag{3.32}$$

Equation (3.32) states that in the discrete world the mapping induced by the operator has to be recast into the original grid representation.

In general, the application of an operator to a state vector will scale as $O(N_g^2)$. For large grid applications, this scaling becomes prohibitively expensive, and much effort must be dedicated to reduce this computation scaling law.

1. Application of local operators

In coordinate space local operators are analytic functions of the coordinate q i.e $\mathbf{A} = f(\mathbf{q})$. The mapping induced by local operators on a coordinate based grid is straightforward. For example, the application of the potential operator:

$$\phi \;=\; \mathbf{V}\psi \;\;\Longrightarrow \phi(q_i) \;\;=\; V(q_i)\psi(q_i) \tag{3.33}$$

This means that the operator $\mathbf{V}$ is diagonal in the grid representation. The application of local operators reduces the operation count of the operator mapping from $O(N_g^2)$ to $O(N_g)$.

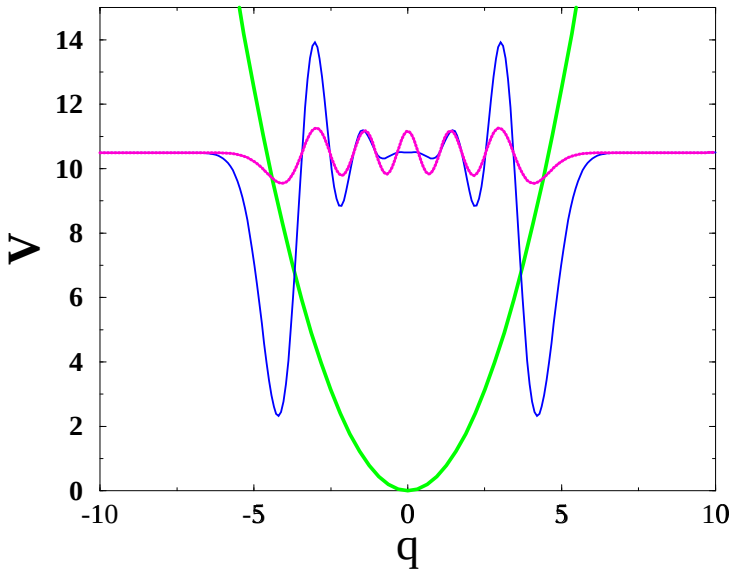

FIGURE 3.4 The mapping created by the potential operator: The wavefunction $\psi(q_i)$ (dashed) the potential function $V(q_i)$ and the mapped wavefunction $\phi(q_i) = V(q_i)\psi(q_i)$(solid). Notice that the potential amplifies certain parts of the wavefunction ψ. (The $n = 10$ eigenstate of the harmonic oscillator is shown.)

From a different perspective the matrix elements of $\mathbf{V}$: $< \psi|\mathbf{V}|\phi >$ are calculated by a quadrature formula where the grid points become sampling points. If the potential operator has discontinuous derivatives, its mapping will reduce a wavepacket to a wavefunction possessing a nonlocal representation in momentum space; i.e if ψ is a band limited function then $\phi = \mathbf{V}\psi$ is not. A typical example is a particle in a box.

2. Mapping induced by differential operators

Differential operators constitute the most important class of nonlocal operators. The mapping of the momentum operator $\mathbf{P} = -i\hbar\frac{\partial}{\partial q}$, and the kinetic energy operator $\mathbf{T} =$

$\mathbf{p}^2/2M = -\frac{\hbar^2}{2M}\frac{\partial^2}{\partial q^2}$ are of special interest.

The calculation of the derivatives is based on the analytic properties of the interpolation functions $g_n(q)$. This means that they can be differentiated at any point:

$$\frac{\partial \psi}{\partial q} = \sum_{n=1}^{N_g} a_n \frac{\partial}{\partial q} g_n(q) \quad . \tag{3.34}$$

and in particular on the grid points:

$$\frac{\partial \psi}{\partial q}|_{q_i} = \sum_{n}^{N_g} \frac{\partial}{\partial q} g_n(q_i) \sum_{j=1}^{N_g} {G_{nj}}^{-1} \psi_j \tag{3.35}$$

Defining the derivative operator matrix: $\frac{\partial \psi}{\partial q_i} = \sum_{j=1}^{N_g} D_{ij}\psi(q_j)$, it becomes:

$$D = FG^{-1} \tag{3.36}$$

where the matrix F becomes: $F_{nj} = \frac{\partial g_n(q_j)}{\partial q}$ and the matrix G is defined in equation (3.3). In a similar fashion, higher order derivative operators can be defined. This general formula is very flexible but may lead to an operator representation of the momentum and the kinetic energy operators which are not hermitian. The derivative operator can also be obtained by differentiating the direct grid interpolation formula (3.18) on the grid points.

An improved derivative formula can be obtained if the derivative of the basis functions can be recast into the original set i.e.:

$$\frac{\partial}{\partial q} g_n(q) = \sum_{m=1}^{N_g} d_{nm} g_m(q) \quad , \tag{3.37}$$

or in matrix form: $\frac{\partial}{\partial q}\mathbf{g} = \mathbf{dg}$. Then the derivative operator has the simple form:

$$D = GdG^{-1} \tag{3.38}$$

If the expansion functions are derived from orthogonal polynomials, the matrix $\mathbf{d}$ can be obtained from the recursion relation for the orthogonal polynomials [32]. If there is a fast transform for G, (which is true for the Chebychev polynomial expansion), then applying equation (3.38) will scale as $O(N_g \log N_g)$.

In the Fourier representation, the transformation matrix $G = U_f$, $((U_f)_{jk} = \frac{1}{\sqrt{N_g}} e^{i2\pi jk/N_g})$ is unitary and supplies the means to transform the wavefunction from coordinate to momentum space. Moreover, the expansion functions $g_k(q) = e^{i2\pi kq/L}$ are eigenvalues of the derivative matrix. Therefore, $d_{kk'} = \frac{i2\pi k}{L}\delta_{kk'}$ which leads to the Fourier derivative formula for order n:

$$\frac{\partial^n \psi}{\partial q^n} = U_f d^n U_f^\dagger \tag{3.39}$$

This formula is analogous to the continuous version of the Fourier derivative formula:

$$\frac{\partial^n \psi(q)}{\partial q^n} = \frac{1}{2\pi}\int_{-\infty}^{\infty} (ik)^n e^{ikq}\tilde{\psi}(k)dk \ . \tag{3.40}$$

A physical interpretation of the Fourier derivative formula Eq. (3.39) is obtained by noticing the analogy between the discrete Fourier transform $\mathbf{U_f}$ and the unitary transformation from coordinate to momentum space in quantum mechanics $< p|q >$. In the momentum representation, the momentum operator and kinetic energy operators become local operators. Therefore the generated mapping is just a multiplication, leading to the algorithm for calculating the kinetic energy operator on the grid representation. The first step in the operation is to Fourier transform $\psi(q)$ from coordinate space to $\tilde{\psi}(p)$ in momentum space. ($\mathbf{A} \rightarrow \mathbf{B}$ in figure 3.5). The second step is to multiply the wavefunction by the kinetic energy operator:

$$T(k) = \frac{\mathbf{p^2}}{2m} = \frac{\hbar^2 k^2}{2m} \ . \tag{3.41}$$

The operation on a component of the wavefunction represented in momentum space becomes:

$$\frac{\mathbf{p^2}}{2m}\tilde{\psi}(k) = \frac{\hbar^2 k^2}{2m} a_k \ . \tag{3.42}$$

(designated by $\mathbf{C}$ in figure III F 3). The operation is completed by an inverse Fourier transform ($\mathbf{C} \rightarrow \mathbf{D}$ in figure 3.5).

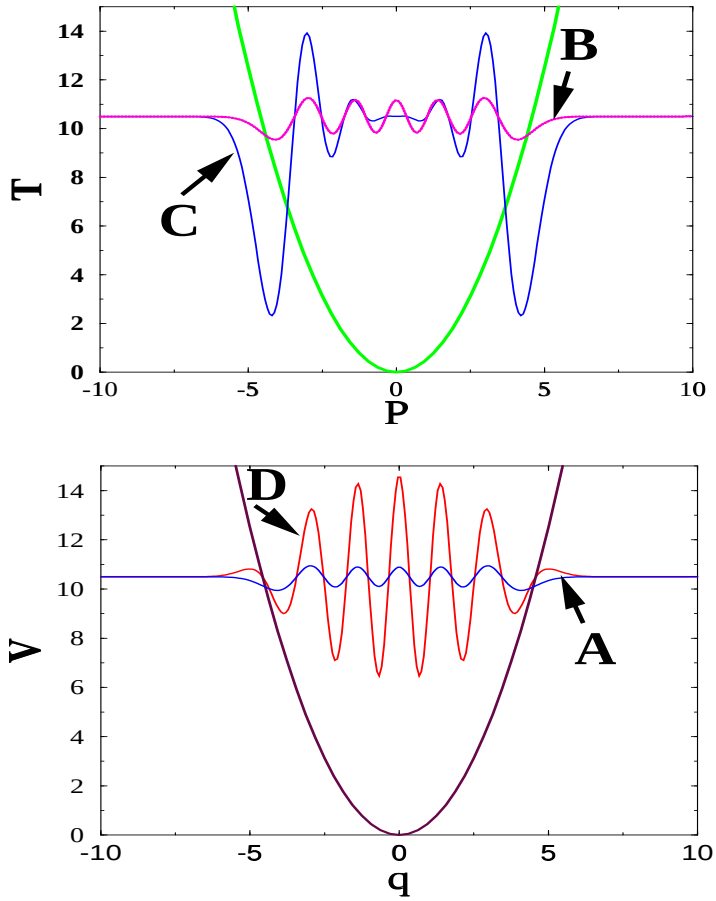

FIGURE 3.5 The four steps in the application of the kinetic energy operator by the Fourier method ($\mathbf{A} \to \mathbf{B} \to \mathbf{C} \to \mathbf{D}$): Lower panel coordinate space. Upper panel momentum space. **A** is the original wavefunction $\psi(q)$. **B** represents the wavefunction in momentum space $\tilde{\psi}(p)$ obtained by Fourier transform of $\psi(q)$. **C** is the application of the kinetic energy operator in momentum space. $\tilde{\phi}(p) = p^2/2M \cdot \tilde{\psi}(p)$ where $T = p^2/2M$ is also shown. **D** is $\phi(q) = \mathbf{T}\psi(q)$. It is the final result obtained by a Fourier transform of **C**.

The operation scaling law of the Fourier method is determined by the forward and reverse unitary transformations from coordinate to momentum space. In general they scale as $O(N_g^2)$ but with the use of the fast Fourier transform (FFT) algorithm this scaling is reduced to $O(N_g \log N_g)$.

The result of equations (3.41) and (3.42) can be generalized for any local operator in momentum space. The algorithm for calculating the mapping of such operators is as follows:

a) calculate the expansion coefficients a_k by the discrete Fourier transform; b) multiply each point in k space by the value of the operator at that point; c) transform the result back to the coordinate sampling space by an inverse Fourier transform.

The convergence of the operator mapping $\phi = \hat{\mathbf{O}}\psi$ is determined by the wavepacket nature of the wavefunction ϕ. The quantum mechanical nature of the approximation depends on the ability to represent the position momentum commutation relation $[\hat{\mathbf{X}}, \hat{\mathbf{P}}] = i\hbar$. A close examination reveals that the function $f(q) = q$ is not band limited on the interval $[0, L]$ because it is discontinuous at the end of the interval $q = L$. Now if $f(q) = q$ is replaced by a periodic function $f(q + L) = f(q)$, then

$$[f(\mathbf{q}), \mathbf{p}] = i\hbar f'(\mathbf{q}) \tag{3.43}$$

since the Fourier method differentiates exactly periodic functions [12]. This means that the Fourier method fulfills the quantum mechanical commutation relations for periodic potentials and compact wavefunctions. Practically this means that converged results are obtained when the wavefunction is effectively zero at the boundaries of the phase space box i.e. it is a wavepacket.

4. Convolution operators

Another important operator which is local in momentum space is the unitary translation operator defined by

$$\hat{\mathbf{U}}_{\mathbf{t}}(y)\psi(x) = \psi(x + y) \ , \tag{3.44}$$

which becomes a phase shift in momentum space:

$$\hat{\mathbf{U}}_{\mathbf{t}}(y)\tilde{\psi}(k) = e^{iky} a_k \ . \tag{3.45}$$

The efficient numerical ability to translate the wavepacket in coordinate space has important consequences. With no loss of accuracy the wavepacket can be centered in the middle of the

grid. This can be done either continuously, resulting in a dynamical grid, or sequentially at predetermined intervals. Such a process can be accompanied by a shift in momentum

$$\hat{\mathbf{U}}_{\mathbf{p}}(k')\tilde{\psi}(k) \;\; = \;\; \tilde{\psi}(k \; + \; k') \; , \tag{3.46}$$

which becomes a phase shift in the coordinate space:

$$\hat{\mathbf{U}}_{\mathbf{p}}(k')\psi(x) \;\; = \;\; e^{ik'x}\psi(x) \; . \tag{3.47}$$

The two shift operator equations (3.44) and (3.46) can reduce significantly the effective volume represented in phase space by matching the grid to regions where the wavefunction has significant amplitude. One should remember that when shifting the wavefunction the potential has to be shifted in the opposite direction and the kinetic energy operator shifts to $\hat{\mathbf{T}}(k) \;\; = \;\; \frac{\hbar^2}{2m}(k-k')^2$. Another use of the shift operator is to interpolate the wavefunction to points which are not represented on the grid. An example of the use of an interpolation procedure is when there is a sudden change of the potential. In photodissociation, for example, the ground state wavefunction is placed on an excited electronic potential which undergoes a rapid momentum increase. To guarantee convergence, the sampling density has to be increased from its value in the ground electronic state.

One simple scheme to effect this interpolation is as follows. Consider a wavefunction which is sampled by N points. It is first transformed to momentum space. Then the wavefunction is cast onto a larger grid of M points by adding $M-N$ zeros to the momentum values for $|k| \; > \; \pi N/L$. A back transform will increase the density of points without adding any new information to the wavefunction.

5. Comparison of different derivative operators

The simple implementation of the translation operator is a consequence of a general property of the Fourier transform that a convolution of two functions in coordinate space becomes a multiplication of the transform function in momentum space. This fact can

be used to study local implementations of the differential operators. In all local methods the derivative matrix D is a banded matrix. For example, consider the mapping of the fourth-order finite difference (FD) kinetic energy operator:

$$\hat{\mathbf{T}}^4_{\mathbf{FD}}\,\psi(q_j) \;=\; -\frac{\hbar^2}{2m}\frac{\psi(q_{j+1}) \;+\; \psi(q_{j-1}) \;-\; 2\psi(q_j)}{\Delta q^2}\;. \tag{3.48}$$

Examining equation (3.48), it is obvious that it is a member of the family of convolution operators and therefore is diagonal in **k** space. Performing a Fourier transform, the spectrum in **k** space of the FD kinetic energy operator is obtained:

$$T_{FD}{}^4(k) \;=\; -\frac{\hbar^2}{2m}\frac{2(\cos(k\Delta q) \;-\; 1)}{(\Delta q)^2} \;=\; \frac{\hbar^2}{2m}\left(\frac{2\sin(k\Delta q/2)}{\Delta q}\right)^2\;. \tag{3.49}$$

Likewise, the sixth-order finite difference operator has the spectrum:

$$T_{FD}{}^6(k) \;=\; -\frac{\hbar^2}{2m}\frac{2\cos(2k\Delta q) - 32\cos(k\Delta q) + 30}{12(\Delta q)^2}\;. \tag{3.50}$$

Figure 3.6 compares the different spectra.

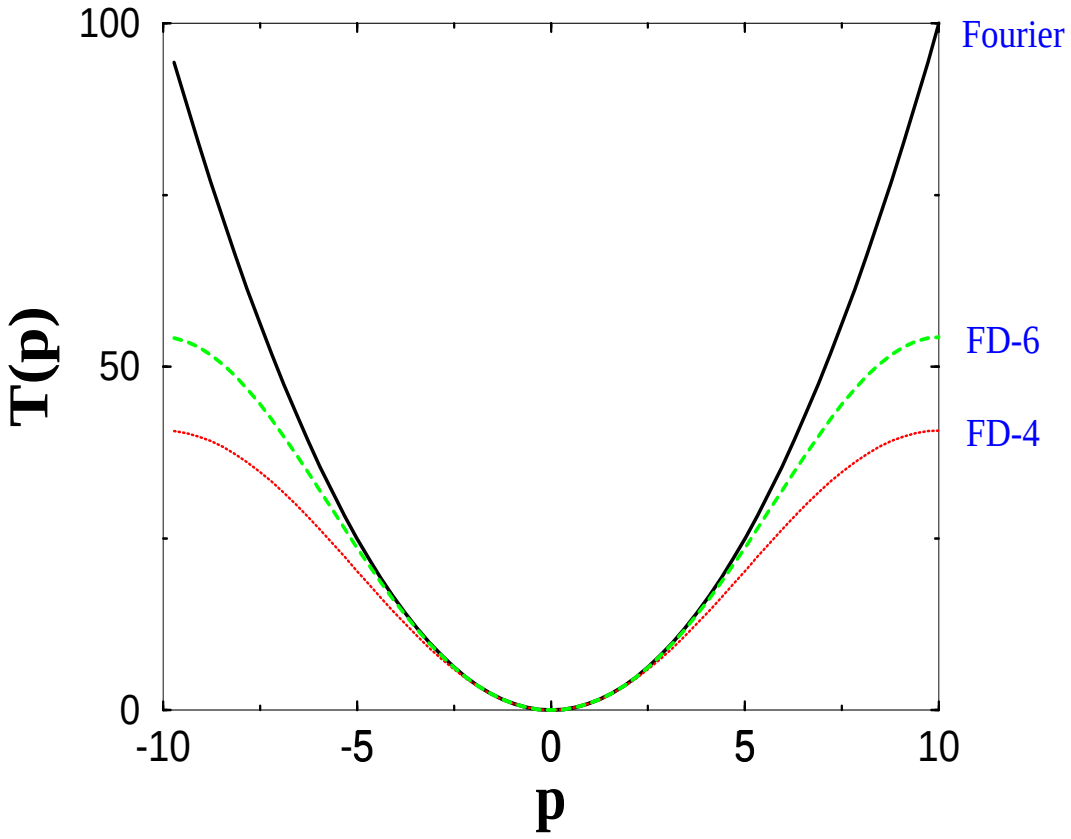

FIGURE 3.6 Comparison of the kinetic energy operator spectrum for the Fourier method (solid) with the fourth-(FD-4) and sixth-order (FD-6) finite difference method.

It is apparent that as the momentum $\mathbf{p}$ increases, the finite difference spectrum deviates more and more from the correct value. It is usually assumed that acceptable accuracy with the FD method is obtained when at least ten points are used per wave period. This means also using ten points per unit volume in phase space. The finite difference algorithms are based on a local polynomial approximation of the wavefunction and therefore the convergence of the method follows a power law of the form $(\Delta q)^n$, where n is the order of the finite difference approximation. This semi-local description leads to a poor spectral representation of the kinetic energy operator, which will be true as well, for other banded representations of the kinetic energy operator such as the recently developed DAF based operator [41]. A general consequence is that a semi-local representation of the momentum operator does not obey the commutation relations of quantum mechanics. This fact, combined with an iterative use of the operator, leads to an exponential accumulation of errors. Propagation with a Hamiltonian based on these operators leads to anomalous dispersion of the wavefunction.

G. The Harmonic Oscillator Example

After reviewing the wealth of considerations used to set up a grid and define the mapping generated by the operators on the grid, a specific example will serve as a summary. The goal is to find the optimal representation of the Hamiltonian operator for the harmonic oscillator $\mathbf{H} = 1/2m\mathbf{P^2} + m\omega^2 q^2$. Figure 3.7 displays the phase space picture of the $n = 10$ eigenstate of the harmonic oscillator. It is apparent that the amplitude of the wavefunction outside the circle $(\frac{1}{2}(q^2 + p^2) = 10 + \frac{1}{2}$ becomes exponentially small, thus, the wavefunction is a wavepacket. Therefore a finite representation based on a Fourier grid will have exponential convergence.

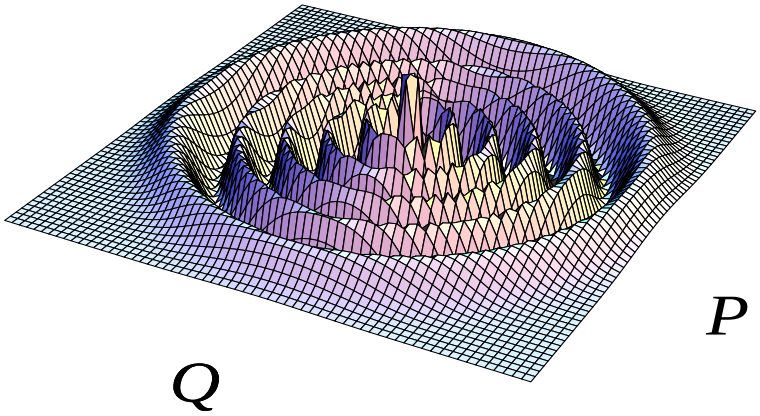

FIGURE 3.7 Wigner distribution function of the $n = 10$ eigenfunction of the harmonic oscillator. The picture shows the extent of the wavefunction in phase space which has nearly optimal sampling due to the balance between the representation of the kinetic and potential energy.

In constructing an optimal grid, the first step is to set the energy cutoff of the system. For a symmetric grid of length L the maximum value of the potential energy is determined by the extreme points on the grid

$$V_{max} = \frac{m\omega^2}{2}\left(\frac{L}{2}\right)^2 = \frac{m\omega^2\Delta q^2 N_g^2}{8}, \tag{3.51}$$

where N_g is the number of sampling points and the grid is centered at about zero. The maximum kinetic energy is limited by the maximum momentum which can be represented on the grid leading to:

$$T_{max} = \frac{P_{max}^2}{2m} = \frac{\hbar^2}{2m}\left(\frac{2\pi}{2\Delta q}\right)^2 = \frac{\hbar^2\pi^2}{2m\Delta q^2} \tag{3.52}$$

Equations (3.51) and (3.52) represent an energy cutoff due to the discrete representation of the Hilbert space. The optimal representation balances the kinetic and potential energy. Using the viral theorem for the harmonic oscillator, the cutoff in the potential energy should match the cutoff in the kinetic energy, with the resulting optimal grid spacing

$$\Delta x_{opt} = \left(\frac{h}{m\omega N_g}\right)^{\frac{1}{2}} . \tag{3.53}$$

Figure 3.8 shows a schematic representation of the phase space representation imposed by the optimal and suboptimal grids.

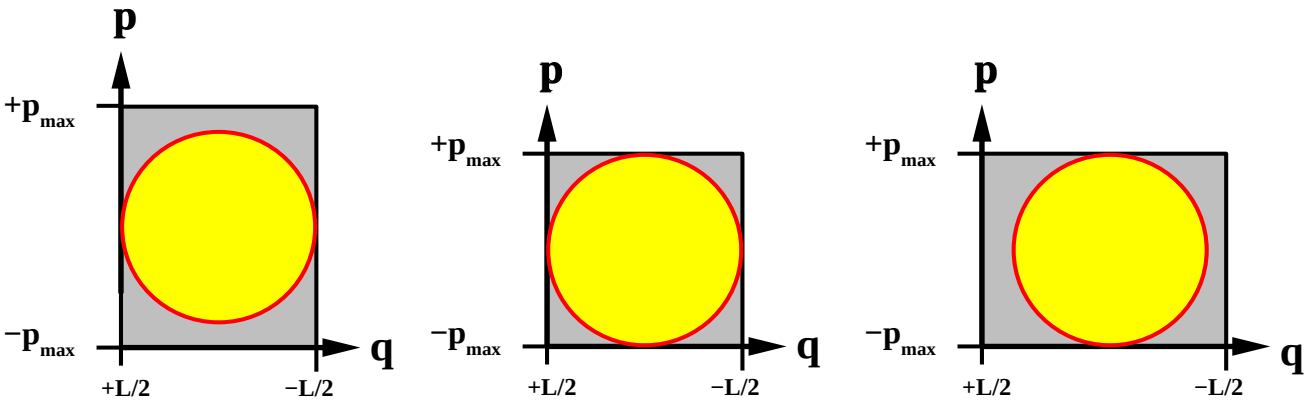

FIGURE 3.8 Schematic representation of the phase space "volume" represented by the Fourier grid. Superimposed is the maximum energy cutoff circle. The grid representation on the left is suboptimal due to an over sampling of the kinetic energy (Δq is too small), and the grid phase space on the right over samples the potential energy (L is too large). The grid in the center shows optimal sampling efficiency of $\pi/4$. which is the ratio of the area of the energy conservation disc to the area of the phase space square.

To illustrate these considerations, a grid is constructed using the functions $\psi(q_j) = \delta(q_i - q_j) = \frac{1}{\pi} sinc(2\pi(q_i - q_j)/\Delta q)$. ($sinc(z) = \sin(z)/z$). This basis function is zero on all other grid points except j, where its value is one. The Hamiltonian matrix in this base is calculated as follows: The potential energy matrix is diagonal : $V_{jj} = V(q_j)$. To calculate the kinetic energy matrix elements, a discrete Fourier transform is applied to the

expansion function ψ_j, then multiplied by $\hbar^2 k^2/2m$ and back transformed. The resulting vector becomes the matrix element T_{ji}. At this stage the Hamiltonian matrix $\hat{\mathbf{H}} = \hat{\mathbf{T}} + \hat{\mathbf{V}}$ is diagonalized and the eigenvalues of the discrete representation are compared to the exact results.

Table I which follows, shows the calculated eigenvalues using 8, 16 and 32 sampling points with the optimal grid spacing Δq_{opt} for $\omega = 1$, $m = 1$,and $\hbar = 1$.

TABLE I. Convergence of the Fourier representation for the harmonic oscillator

N_g	Exact	8 points	16 points	32 points
Δq_{opt}		0.8862265	0.6266568	0.4431132
1	0.5	0.4999760107111692	0.4999999998715793	0.4999999999999845
2	1.5	1.500539183698194	1.500000006153576	1.499999999999986
3	2.5	2.494397791604125	2.499999857637178	2.500000000000002
4	3.5	3.534291735531325	3.500002068787167	3.499999999999993
5	4.5	4.378294841394608	4.499978178076544	4.499999999999982
6	5.5	5.960743369677700	5.500169240572392	5.500000000000130
7	6.5	6.212358517586826	6.498928884935602	6.499999999997876
8	7.5	9.976917743504451	7.505122466888302	7.500000000025498
9	8.5		8.478529454896226	8.499999999731434
10	9.5		9.567379412999802	9.500000002414588
11	10.5		10.33263329166096	10.49999998073345
12	11.5		11.95570264326039	11.50000013337068
13	12.5		12.04789296489282	12.49999916184023
14	13.5		14.56012875187433	13.50000457741937
15	14.5		15.44949561677325	14.49997680742042
16	15.5		20.69252130835984	15.50010120025324
17	16.5			16.49957859092886
18	17.5			17.50146417275678

When the results for 8 sampling points are compared with 16 sampling points, the exponential convergence of the expansion is demonstrated. For the ground state energy the error decreases six orders of magnitude by only doubling the number of grid points. Other states show similar behavior. When the number of points is doubled again to 32, the error in the ground state becomes saturated because the roundoff error of the double precision arithmetic used in the calculation overcomes the representation error. For unsaturated eigenvalues doubling the number of points from 16 to 32 reduces the error another five to six orders of magnitude.

Another view on the convergence of the Fourier method can be obtained by counting the number of converged eigenvalues obtained for N_g grid points. If the convergence criterion is three significant digits, it is observed that 3 converged eigenvalues are obtained for $N_g = 8$, 8 for $N_g = 16$, and 20 for $N_g = 32$ grid points. This means that the fraction of significant eigenvalues increases with the number of points in the representation. Figure 3.9 shows the fraction of significant eigenvalues as a function of the logarithm of the number of points.

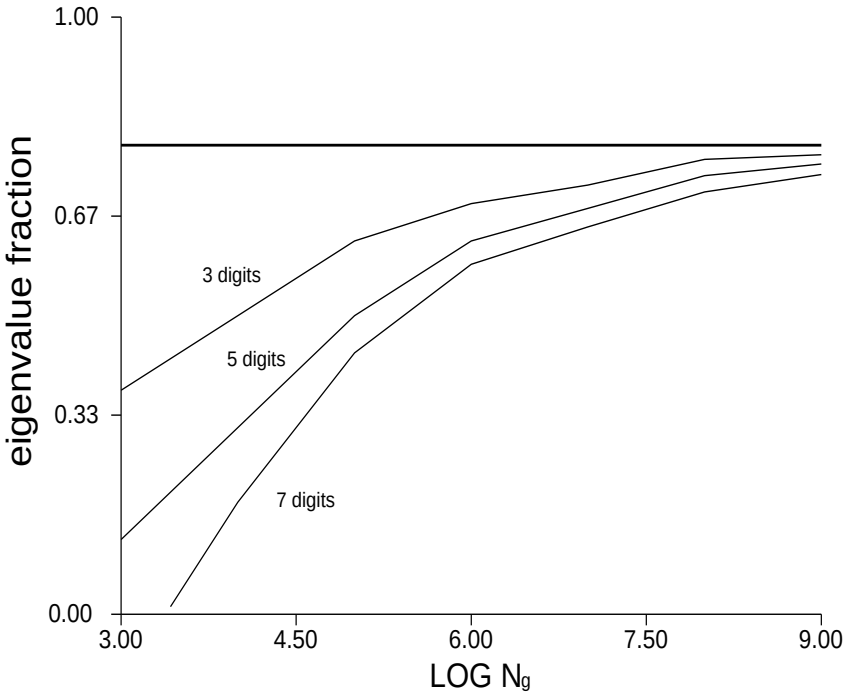

FIGURE 3.9 Sampling efficiency defined by the ratio of converged eigenvalues within a fixed number of digits to the number of sampling points, as a function of the logarithm of the number of sampling points. The heavy line represents the asymptotic value of $\pi/4$.

Figure 3.9 shows that the converged eigenvalue fraction increases with the number of points until it reaches saturation regardless of the number of significant digits used as the convergence criterion. This asymptotic ratio can be used to define the sampling efficiency.

The saturation of the eigenvalue fraction occurs because the Fourier method constructs a rectangular phase space (see figure 3.7). Using the balanced choice of Δq_{opt}, the phase space becomes a square. On the other hand, due to energy conservation, the support for an eigenfunction in phase space up to a cutoff energy has the shape of a disc determined by the largest eigenfunction. (or an ellipse in the general case). The area between the circumference

of the disc and the perimeter of the square is wasted sampling space. Therefore the maximum sampling efficiency is the ratio of the area of the circle to the area of the square leading to $\pi/4 \approx 79\%$. This is the asymptotic value represented by the bold line in Figure 3.9 .

To illustrate this point further, Figure 3.10 shows the converged eigenvalue fraction as a function of the grid spacing Δq. It is clear that a square in phase space offers the optimal choice where, to the left of the cusp point $\Delta q = \Delta q_{opt}$, the kinetic energy operator error dominates. To the right of the cusp point, the potential energy error dominates.

This example shows that a careful choice of grid parameters which balance the representation of the kinetic and potential energy can drastically reduce the amount of computation effort.

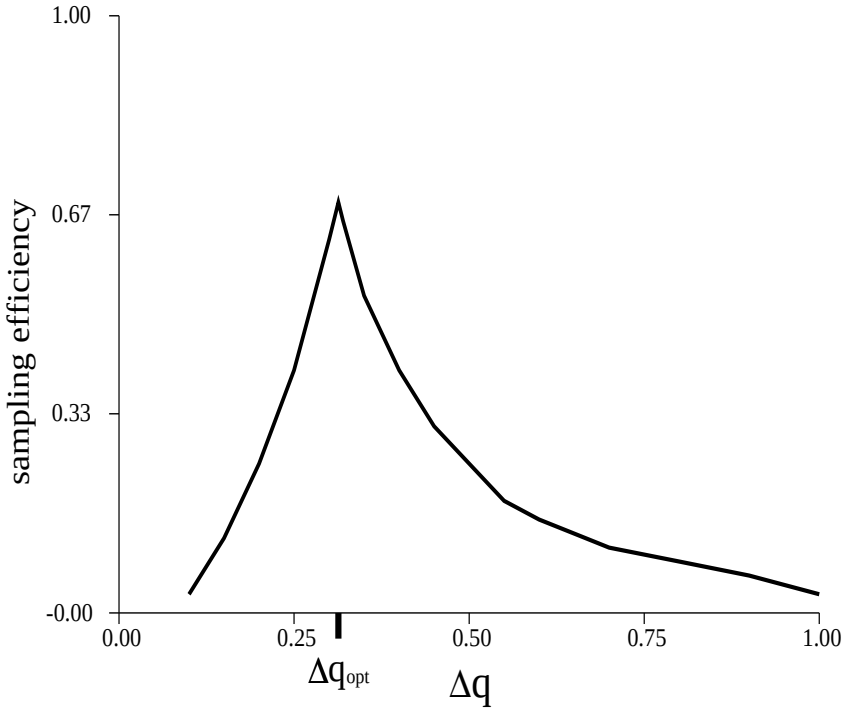

FIGURE 3.10 Sampling efficiency defined as the ratio of converged eigenvalues divided by N_g, for a fixed number of points ($N_g = 64$) as a function of the grid spacing Δq. The optimal sampling spacing is

marked. At Δq_{opt} the sampling efficiency approaches $\pi/4$ at the cusp point Δq_{opt}.

Table II below shows the convergence of the first eigenvalues of the finite difference method for the same parameters as table I. The kinetic energy spectrum was constructed from equation (3.49). The grid spacing Δq was optimized for each case independently.

TABLE II. Convergence of the Finite Difference representation for the harmonic oscillator

Fourth order FD					
N_g	Exact	8 points	16 points	32 points	64 points
Δq_{opt}		0.7	0.4	0.2	0.11
1	0.5	0.4825740879	0.49478668002	0.49860380104	0.499603845744
2	1.5	1.4317143539	1.47679543400	1.49594408176	1.498464505411
3	2.5	2.2214522909	2.41491682858	2.46274206266	2.490855167811
4	3.5	3.1888159106	3.43350682128	3.54493542145	3.511444750027
5	4.5	3.5308260773	4.10115403608	4.21270019153	4.381333406923
6	5.5	4.4614149311	5.56420368670	5.96798953995	5.712163111633
Sixth order FD					
N_g	Exact	8 points	16 points	32 points	64 points
Δq_{opt}		0.75	0.44	0.24	0.13
1	0.5	0.496832961	0.4996361441	0.4999643185	0.4999968936
2	1.5	1.485276212	1.4982057984	1.4998077039	1.4999837996
3	2.5	2.393088218	2.485823514	2.4985394570	2.4998518646
4	3.5	3.439160266	3.5084173131	3.5020862644	3.5004457190
5	4.5	3.920284648	4.3402199322	4.4695728153	4.4948505331
6	5.5		5.7031594608	5.5688982555	5.5178475240
7	6.5		6.0977450000	6.2657050814	6.4167645240

Table I and Table II reveal the slow convergence of the finite difference method compared to the Fourier method. Even for the sixth order finite difference, the convergence is increased only one order of magnitude when the number of points is doubled. Also, the finite difference method uses a much smaller optimal grid spacing than the Fourier method: for $N_g = 64$, $\Delta q_{opt} = 0.313$ in the Fourier method compared to $\Delta q_{opt} = 0.11$ in the FD-4 method and $\Delta q_{opt} = 0.13$ in the FD-6 method. This means that the FD method has a much smaller sampling efficiency. These results are typical of the FD method. Moreover since grid methods are used in an iterative fashion these errors accumulate.

H. Mapped Fourier Methods

The global balancing of kinetic and potential energy was shown to be an important step in optimizing the calculation. However, even for the optimally balanced representation of the harmonic oscillator there is "air" between the rectangular "box" in phase space used by the Fourier method and the circular shape defined by the Hamiltonian. One can imagine cases where the phase space box has a more complicated shape. For example, it can be expected that the optimal sampling density of the Morse oscillator should be lower in regions of small classical kinetic energy.

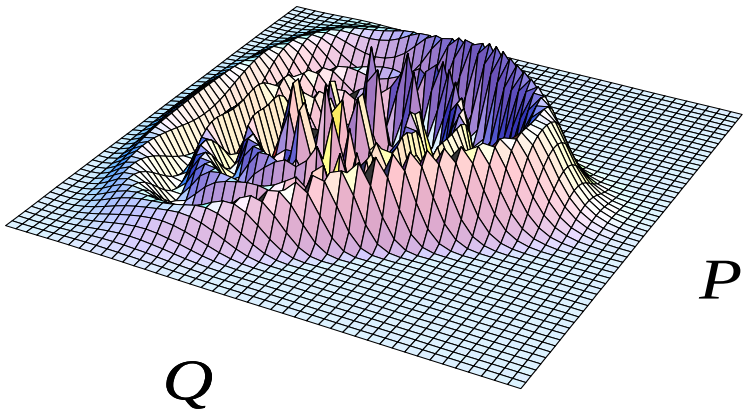

FIGURE 3.11 Phase space representation of the $n = 8$ vibrational eigenstate of H_2. Notice that at the outer classical turning point, the momentum distribution becomes narrow due to the slowing down of the "particle" at the outer region of the potential. Notice the unused phase space area for large p and q. volume

A solution to the balancing problem is to define a mapping transformation which correlates the position and momentum. This is achieved by transformation from the original set of coordinates q to a new set q', the curvilinear coordinate:

$$\bar{q}_j = M_j(\{q_i\}, \alpha) \tag{3.54}$$

and the inverse transformation

$$q_j = M_j^{-1}(\{\bar{q}_i\}, \alpha) \tag{3.55}$$

where α is a set of parameters defining the mapping function M.

The new space is defined in terms of the Riemannian metric tensor (g_{ij}) (we use the summation over repeated indices convention):

$$g_{ij} = \frac{\partial q^k}{\partial \bar{q}^i}\frac{\partial q^k}{\partial \bar{q}^j} \tag{3.56}$$

The operator of Laplacian is:

$$\nabla^2 = J^{-1}\frac{\partial}{\partial \bar{q}^j}\left(J\ g^{jk}\frac{\partial}{\partial \bar{q}^k}\right) \quad ; \quad J = \sqrt{|det\,(g_{ij})|} \tag{3.57}$$

where g^{jk} is the jk matrix element of the metric tensor inverse matrix and J is the Jacobian of the transformation. The operator of integration:

$$\int \psi(\{q_i\}) \prod_{j=1}^{N} dq_j = \int \psi\left(\{\bar{q}_i\}\right) J \prod_{j=1}^{N} d\bar{q}_j \tag{3.58}$$

The result of this mapping is that a correlation is induced between the kinetic and potential operators. In the mapping procedure the kinetic energy operator is calculated by the chain rule:

$$\hat{\mathbf{T}} = -\frac{\hbar^2}{2m}\left(\frac{\partial M}{\partial q}\right)\frac{\partial}{\partial q'}\left(\frac{\partial M}{\partial q}\right)\frac{\partial}{\partial q'} = \frac{\hbar^2}{2m}\left(J^{-1}\frac{\partial}{\partial q'}\right)^2 \tag{3.59}$$

This kinetic energy operation can be implemented by a sequential evaluation of the first derivative multiplied by J^{-1}. The overall evaluation requires at least three Fourier transforms per operation compared to two Fourier transforms for the simple, rectilinear, Fourier method.

There are many examples of such mapping functions. For example if

$$\theta = \cos^{-1}(q) \tag{3.60}$$

and

$$q = \cos(\theta)\ , \tag{3.61}$$

then the Fourier method is transformed into a Chebychev pseudo-spectral representation [19]. This representation which belongs to the class of orthogonal polynomial transformations is exceptional because the mapping of equation (3.61) has a fast transform implementation.

Another example is the mapping of the interval $-L/2 < q < L/2$ into itself [42]:

$$q \;=\; M^{-1}(q', \alpha, \beta) \;=\; \frac{L}{2} D \left[\frac{q'}{L/2} \;-\; E\alpha \tan^{-1}\left(\frac{q'}{\alpha L/2} \right) \right] \tag{3.62}$$

where:

$$D(\alpha, \beta) \;=\; \frac{1}{1 - (1-\beta)\alpha \tan^{-1}(\frac{1}{\alpha})} \tag{3.63}$$

$$E \;=\; 1 - \beta \tag{3.64}$$

where α and β are external parameters used to adjust the function to the problem. Figure 3.12 shows the mapping transformation used to enhance the sampling at the origin which is effective for a Coloumbic problem.

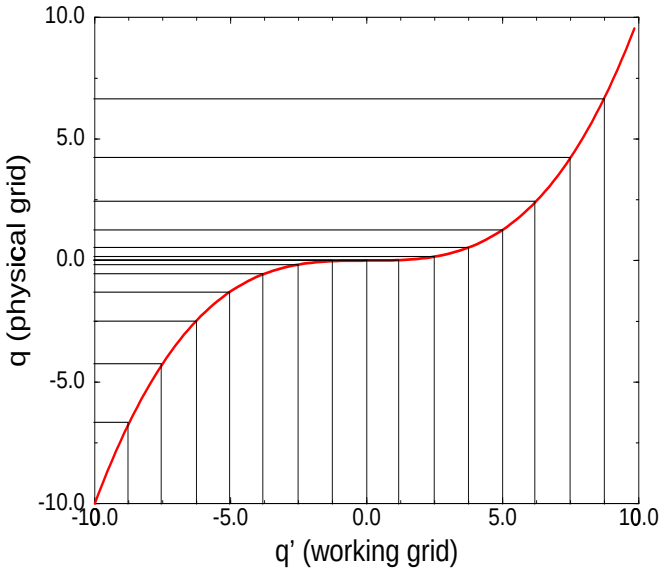

FIGURE 3.12 The mapping transformation: the relation between the physical grid and the working grid using the mapping function in equation (3.62) with the parameters $\alpha = 0.00005$, $\beta = 9$. Notice the

congesting of sampling points near the origin which is appropriate for the Coulomb problems.

The above mapping procedure was tested on the hydrogen atom eigenfunctions. In all cases the mapping procedure was able to enhance the convergence as is demonstrated in Fig. 3.13 .

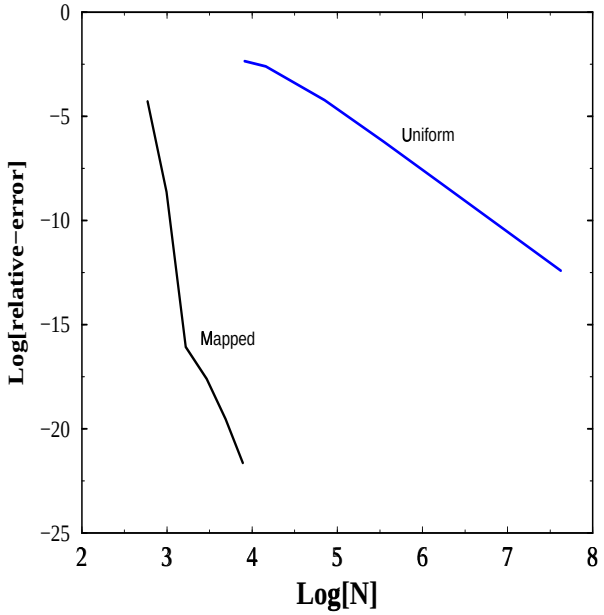

FIGURE 3.13 The convergence of the energy of the first excited state of hydrogen $\psi(r) = r^2 e^{-r/2}$, as a function of the number of grid points N_g. It is clear that the mapped grid increases the sampling efficiency and therefore increases the energy accuracy by many orders of magnitude.

The mapping transformation is straightforwardly extendible to multi-dimensions [43]. In variational calculations, for example in the finding of the ground state wavefunction, the optimal mapping parameters can be obtained variationally [44].

The concept of a functional space which contains a local representation of the kinetic energy operator can be carried beyond Cartesian coordinates. For example the kinetic energy operator in radial coordinates becomes:

$$\frac{\hat{\mathbf{P}}_{\mathbf{r}}^{\mathbf{2}}}{2m} = -\frac{\hbar^2}{2m}\left[\frac{1}{r^2}\frac{\partial}{\partial r}r^2\frac{\partial}{\partial r}\right] . \tag{3.65}$$

In the Fourier method this kinetic energy operator is a special case of mapping as described in the section III H [42,45]. An alternative method for the radial part is based on the fact that the Bessel function $J_{1/2}(r)$ is an eigenfunction of the radial part of the Laplacian. This means that by using a Bessel transform, the radial part of the Laplacian becomes a local operator with the spectrum $-k^2$. This result can be generalized by using the transform with $J_{l+1/2}$. In this case a centrifugal part $l(l+1)/r^2$, is included in the transformation [46,47].

There are two approaches to this problem. The first, which is in the spirit of the DVR scheme, is to use the zeros of the Bessel function $J_\nu(r) = 0$ as collocation points. It has been shown by Lemoine [47] that this procedure leads to an almost unitary collocation transformation. The second approach is based on the fact that technically, fast Bessel transforms can be carried out by a change of variable. The transform becomes a convolution which is then carried out by means of a fast Fourier transform [48–50]. The Fourier-Bessel transform of order ν is defined by:

$$\hat{\psi}(k) = \int_0^\infty r\psi(r)J_\nu(kr)dr \tag{3.66}$$

for $k > 0$. The Bessel transform is its own inverse. Substituting $r = r_0e^{-y}$ and $k = k_0e^x$ in equation (3.66) and multiplying both sides by $e^{\alpha x}$ gives:

$$e^{\alpha x}\hat{\psi}(k_0e^x) = r_0^2\int_{-\infty}^{\infty} e^{(\alpha-2)y}\psi(r_0e^{-y})e^{\alpha(x-y)}j_\nu(r_0k_0e^{x-y})dy . \tag{3.67}$$

The expression on the right hand side is a convolution of the function $e^{(\alpha-2)y}\psi(r_0e^{-y})$ and $r_0^2e^{\alpha x}J_\nu(r_0k_0e^x)$. The parameter α is arbitrary and therefore can be chosen to optimize the accuracy. The convolution theorem [51,24] states that the Fourier transform of the

convolution of b and c, denoted $b * c$, equals the product of their Fourier transforms. Hence $b * c$ can be computed by performing an FFT on b and c, multiplying the results, and performing an inverse FFT. The use of the Fourier-Bessel transform can be viewed as a logarithmic mapping function on the coordinates r. Numerical tests show [47] that the grid based on the zeros of the Bessel function has improved sampling efficiency over the mapping convolution transformation.

J. Symmetry adopted grids

An obvious solution to minimize the number of grid points N_g is to introduce symmetry. Consider for example an inversion point such as the point $x = 0$ in the harmonic oscillator. The eigenfunctions can be classified as being either even or odd with respect to parity: $\psi(q) = \pm\psi(-q)$. If one restricts the calculation to one class of functions the computational effort can be reduced by a factor of two by using a fast cosine transform for even functions and a fast sine transform for odd functions [52]. The same symmetry considerations should work for other types of grids.

Translational symmetry of the type $\hat{\mathbf{V}}(q + nL) = \hat{\mathbf{V}}(q)$ can also be exploited. The symmetry of the potential is reflected in selection rules imposed on the momentum change. A typical example can be found in atom scattering from a crystal surface. In this case the selection rule $\Delta k = \pm n\pi/L$ is imposed. By matching the grid to the unit cell and employing the periodic boundary conditions of the Fourier representation, the selection rules are automatically fulfilled. In more than one dimension the matching of the grid to the unit cell might require a skewed grid representation. As will be seen in subsection IV C, the skewed grid has more efficient sampling. Other types of symmetry can be considered by working out the selection rules on Δk. Then the kinetic energy operator can be evaluated by shifting the spectrum in k space using equation (3.47). The details can be found in reference [53].

IV. MULTIDIMENSIONAL GRIDS

A. Direct product grids

A straightforward approach to constructing a multi-dimensional representation is to assemble it directly from a direct product of one-dimensional representations. On a grid this means that the position vector $\mathbf{q}$ becomes $q_{ijk...} = \{q_i^1, q_j^2, q_k^3, ...\}$ where q_l^n is the n'th one dimensional position pointer. Such a construction has the advantage that each degree of freedom is independent thus allowing each individual representation to be optimized. Naturally, the optimizations leads to different types of grids for each degree of freedom. For example, in circular coordinates, a possible choice is an evenly spaced grid in the angle ϕ and a grid in the radial coordinate r.

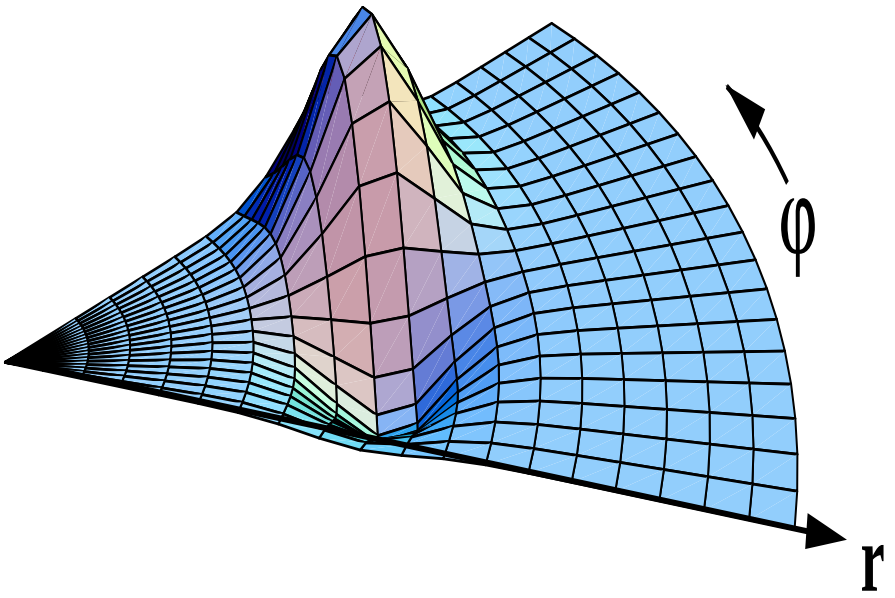

FIGURE 4.1 A direct product representation in r and ϕ coordinates of a wavefunction representing a collinear encounter in hyperspherical coordinates

A more elaborate example of a multi-dimensional representation is the grid construction in molecular surface scattering [54–59]. It is constructed from a three-dimensional Fourier grid for the translational $\{x, y, z\}$ coordinates and a spectral expansion using spherical harmonics for the angular coordinates θ and ϕ and a DVR type grid for r. The translational grid spacing in the x and y coordinates is matched to the unit cell of the crystal surface.

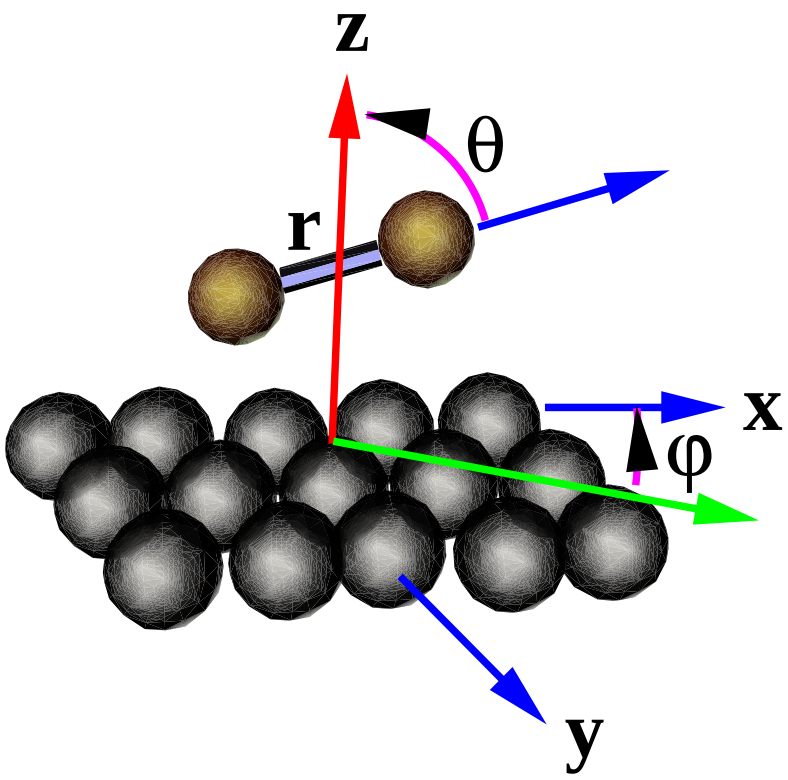

FIGURE 4.2 The grid and coordinate setup for a molecular surface scattering encounter. A Fourier grid is used for the x, y, z coordinates and a spectral expansion for the θ, ϕ coordinates.

Since the propagation is carried out in the global time-energy phase space, it imposes a common energy cutoff on all the individual degrees of freedom; otherwise the representation is not balanced.

The advantage of the direct product construction is the flexibility in adopting the representation to each specific degree of freedom. The drawbacks of the direct product con-

struction are obvious. The energy range becomes N times larger for N degrees of freedom. Moreover there is more chance for empty sampling space. For example in the H_2+H encounter once the energy band is restricted there are regions in coordinate space which are well into the classical forbidden region where the wavepacket amplitude is negligible. Figure 4.3 shows a rectangular grid for H_2+H encounter superimposed on the potential. This situation becomes more acute in higher dimensions.

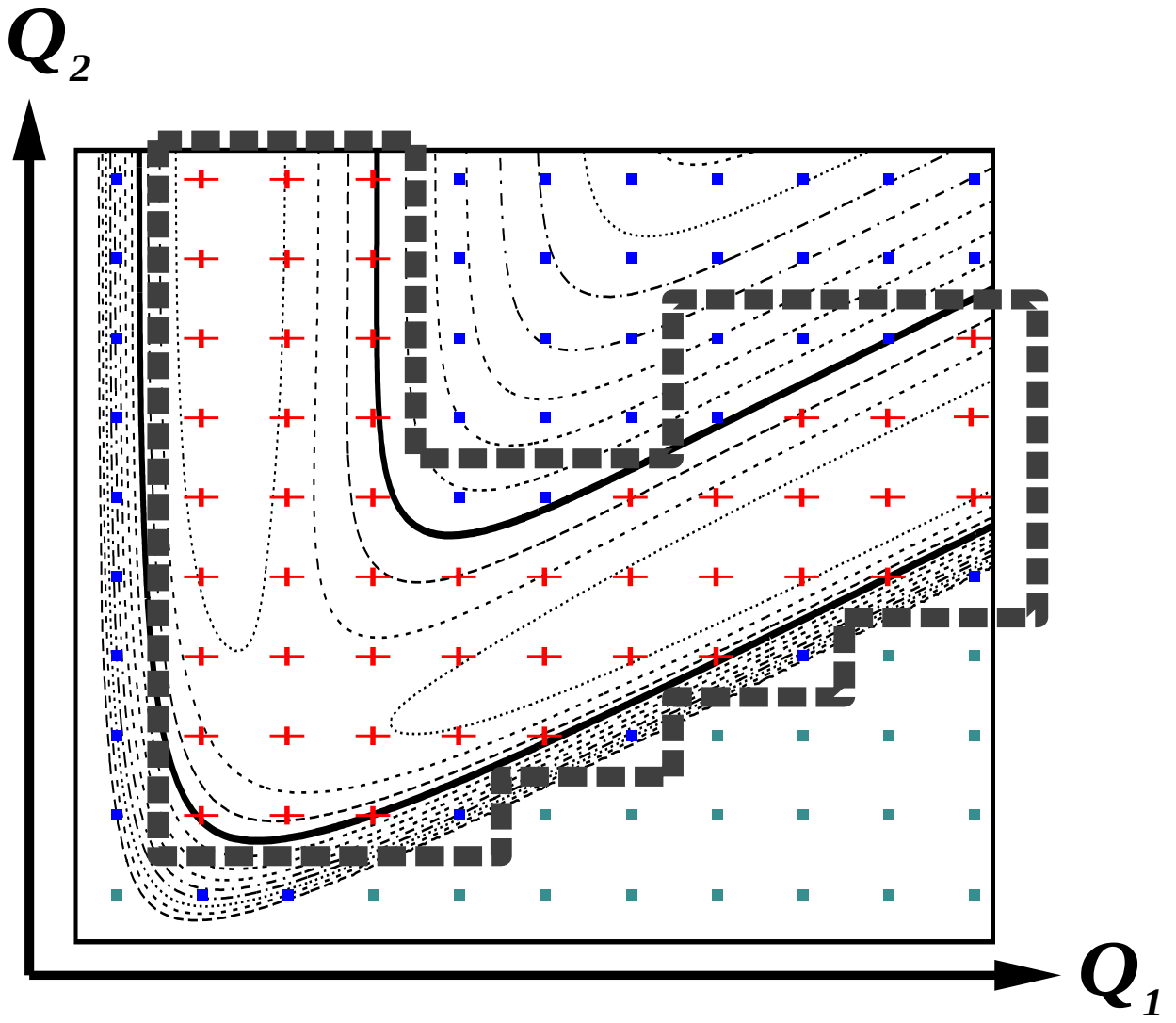

FIGURE 4.3 A two dimensional rectangular grid for the collinear H_2+H encounter in mass scaled Jacobi coordinates superimposed on the potential. The thick contour line represents the potential energy cutoff. The grid points represented by + signs have potential energy less than the cutoff value. The gray grid points are in the forbidden region where the internuclear distance r_2 is negative. The dashed line represents

the border of a rectangular correlated grid. The number of grid points correlated by a cutoff energy is 44% of the total number N_g and the number of correlated rectangular grid points is 53% of the total number.

B. Simple correlated grids

Representation methods are designed for wavepackets. It is therefore safe to assume that the wavepacket decays exponentially when entering the classical forbidden region of phase space. In the position picture, grid correlation can be obtained by eliminating grid points which are above a certain potential energy cutoff value [60]. The retained points below an energy cutoff are marked in Fig. 4.3 . In many cases this procedure can reduce the number of grid points significantly but the price will be a complicated grid topology. A compromise which allows the use of the FFT algorithm is to decompose the grid into rectangular boxes. Such a construction is represented in Fig. 4.3 by a thick dashed line. The values of the points between the energy restricting contour and the grid boundary can be replaced by zero, thus maintaining the ability to use the FFT algorithm while minimizing the energy range. The first application of grid methods to reactive scattering [7] eliminated part of the high energy three body dissociation region by constructing an **L** shaped grid.

A more involved situation is found in curvilinear coordinates. For example, in circular coordinates the angular kinetic energy term $\mathbf{T} = \frac{1}{2mr^2}\frac{\partial^2}{\partial\phi^2}$ correlates the angular kinetic energy with the radial coordinate r.

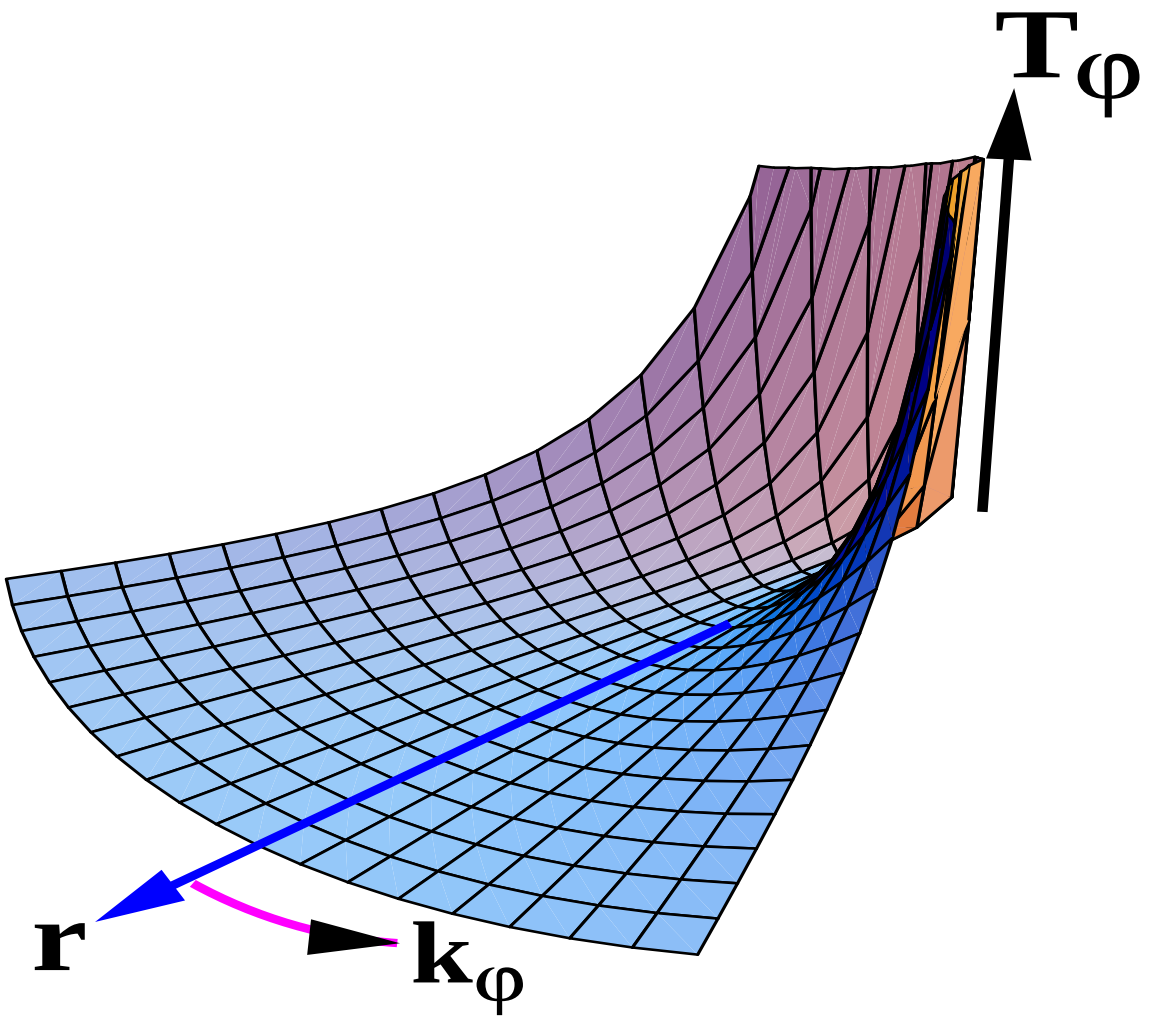

FIGURE 4.4 The kinetic energy operator $T_\phi = \hbar^2 k_\phi^2 / 2mr^2$ in angular momentum space, as a function of r and k_ϕ for hyperspherical coordinates. Notice that the energy cutoff is a function of both variables.

The above observation suggests imposing an energy cutoff on the angular momentum. As a consequence, as r approaches the origin, the number of expansion functions becomes smaller than the number of grid points in ϕ.

Grid constructions in which the number of grid points is unbalanced with the number of expansion functions is common in situations where a high degree of correlation is needed. As described above, grid points are eliminated which are deep in classically forbidden regions.

This amounts to replacing the value of the wavefunction at these points by zero. These considerations can be applied to the momentum space, leading to the elimination of expansion functions which are above the energy cutoff i.e. are in the classical forbidden region in momentum space. The result is a highly correlated grid. If the points and functions are related by a quadrature rule the elimination of points or functions causes no problem in principle since the transformation from the point to the functional representation is still unitary.

If the functional base is already correlated, i.e not a direct product type, a more complicated grid construction results. An important example is the $Y_{lm}(\theta, \phi)$ functional representation in spherical coordinates where the θ expansion function is correlated with ϕ through the angular momentum projection m [61]. Corey and Lemoine [62,35] have suggested use of a direct product grid in θ and ϕ where the grid points in θ are Gaussian quadrature points of Legendre polynomials of degree j_{max}. These points are able to integrate exactly the associate Legendre polynomials of order less than $2j_{max}+1$. In such a construction there are more grid points than expansion functions, but due to the quadrature rule, there is no ambiguity in the transformation from grid points to functions and back.

The adiabatic pseudo-spectral method [63–65] is also based on a similar approach. First a direct product grid is constructed. Then by adiabatic reduction, the spectral functional expansion is reduced by correlating in a hierarchical form each degree of freedom successively. As a result, the number of grid points becomes larger than the number of functions. To relate the two representations, a least square procedure [18] is employed to transform from the grid to the functional representation. The result is a correlated representation which can be used to further optimize the representation by eliminating grid points which are deep in the classical forbidden region. In the next section it will be shown that a non-direct product grid is able to enhance the sampling significantly.

For more general problems, it has been observed that the direct product representation, which for the Fourier method implies a representation by an equally spaced Cartesian grid, is not optimal. A careful analysis of the Fourier method leads to the observation that this direct product grid is not isotropic in momentum space, so that different directions have different sampling intervals. A faithful representation of a multidimensional function by the Fourier method means that the function is band limited. The symmetric construction of the coordinate and momentum representation means that the description of the function is also periodic in momentum space. The representation therefore can be viewed as an infinite number of replicas of the original **k** space picture extending in all directions. The band limited property of the original functions means that these replica do not overlap. If *a priori* there is no preferable direction in space then a cutoff in momentum can be represented as a sphere with radius p_{max}. A Cartesian grid in coordinate space is also Cartesian in momentum space. Therefore the non overlapping role can be envisioned as packing spheres so that they touch their neighbors at $2D$ points for D dimensions. It is clear that the best sampled direction is along the diagonal, but for an isotropic problem the volume between the spheres becomes wasted sampling volume.

Although a completely isotropic grid is not possible, the sampling positions can be chosen to construct the optimum isotropic grid in momentum space. From the previous description it can be concluded that the optimal sampling points are equivalent to the centers of multidimensional densely packed hard spheres. (The problem of the optimal packing of hard spheres has been solved up to 23 dimensions [66]). The free volume between the spheres is wasted sampling volume. The sampling efficiency can be defined as the ratio of the volume of the space-filling spheres to the volume of the total space. Figure 4.5 illustrates the situation in three dimensions.

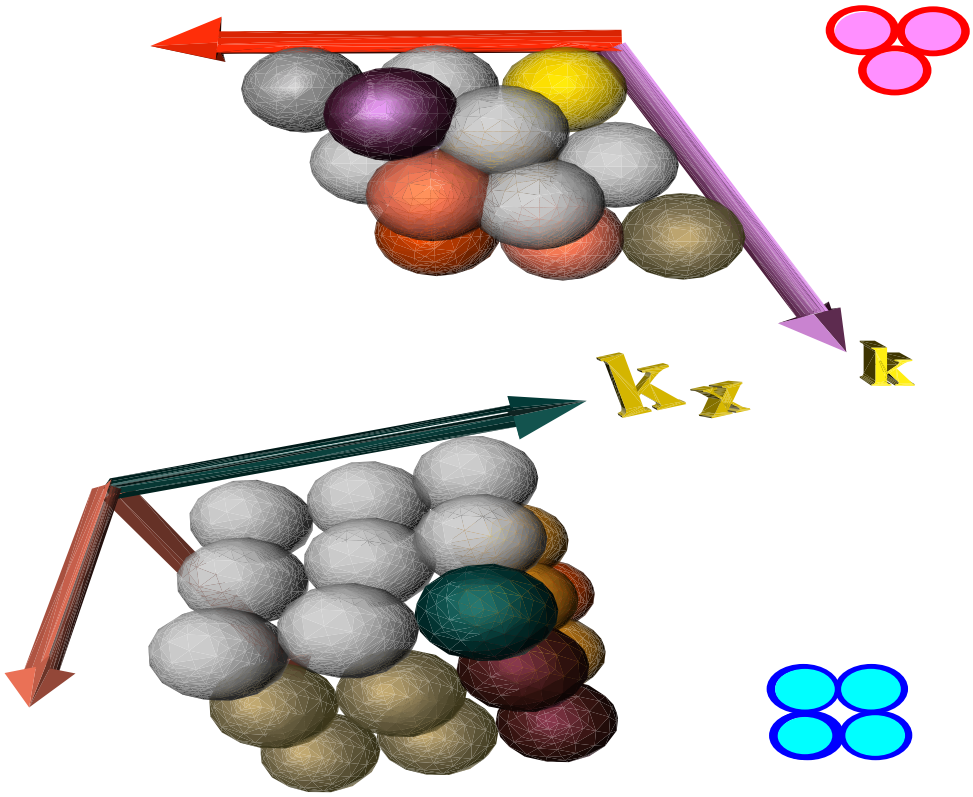

FIGURE 4.5 Schematic view of the k spectrum sampled on a three-dimensional cubic grid (bottom) and on a skewed grid (top). The Fourier transform of a function f is contained in the sphere p_0. Sampling the function f on a discrete grid produces copies of $\bar{f}(K)$, each containing a sphere with radius K_{max}. These spheres should be distinct for optimal sampling.

The Cartesian grid reaches a sampling efficiency of $\frac{\pi}{4} \approx 79\%$, the ratio of the area of a disc to a square. Skewing the grid increases the sampling efficiency to $\frac{\pi}{2\sqrt{3}} \approx 91\%$ the ratio

of a disc to a hexagon. In many dimensions, the limit of one sampling point per unit volume is not obtainable even for optimal packing. Table III compares the sampling efficiency of a cubic grid with the optimal grid as a function of dimension.

TABLE III. Isotropic Sampling Efficiency

Dimension	Maximum Efficiency $\eta_{max}(\%)$	Cubic Lattice η_{cub} (%)	Improvement Factor η_{max}/η_{cub}
1	100.0	100.0	1.0
2	90.7	78.5	1.15
3	74.0	52.4	1.4
4	61.7	30.8	2.0
5	46.5	16.45	2.8
6	37.3	8.07	4.6
7	29.57	3.69	8.0
8	8.07	0.505	16.0

Source: Peterson and Middleton [66].

It can be deduced from Figure 4.6 that the importance of optimal sampling increases with dimensionality. For calculations beyond three dimensions, optimal sampling becomes extremely important. For example, for six dimensions, 2.7 sampling points are needed per unit volume, compared to 12.4 points in the Cartesian cubic lattice. Nevertheless even the optimal sampling efficiency decreases with dimensionality. This fact poses an intrinsic limitation to the Fourier method for multidimensional calculations.

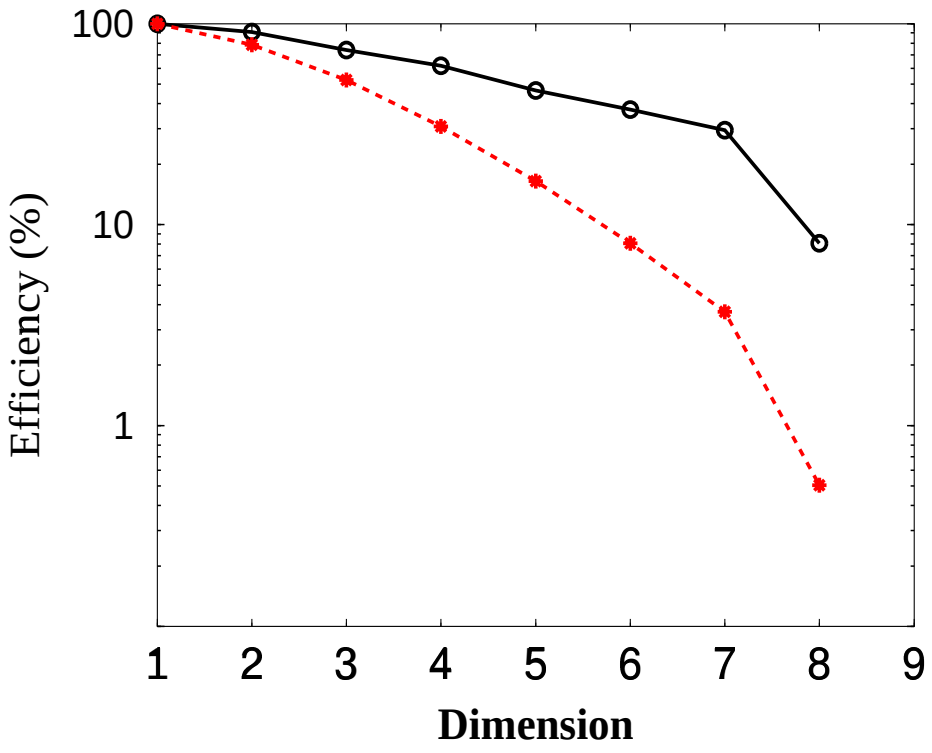

FIGURE 4.6 Comparison of sampling efficiency of a cubic to a skewed grid as a function of dimension. The stars represent the cubic grid, the open circles the skewed grid.

In a rectangular set of multidimensional coordinates, the kinetic energy operator is separable,

$$\hat{\mathbf{T}} = \frac{\hbar^2}{2m} \sum_{i=1}^{D} \mathbf{K_i^2} , \tag{4.1}$$

where $\mathbf{K_i}$ is the vector of k values in the spatial dimension i. In the case of the optimal

packing or in other skewed sets of coordinates, the kinetic energy operator becomes

$$\frac{\hat{\mathbf{P}}^{\mathbf{2}}}{2m} = \frac{\hbar^2}{2m}\mathbf{K}^{\dagger}\cdot\mathbf{G}\cdot\mathbf{K}\,, \tag{4.2}$$

where $\mathbf{K}$ is the vector of k values for each spatial direction and $\mathbf{G}$ a positive definite matrix connecting spatial direction i with direction j. The $\mathbf{G}$ matrix can be calculated by using the knowledge of the coordinates of the centers of the optimally packed spheres [67]. This correlated grid appears naturally in atom surface scattering where the grid is matched to the unit cell. It leads to the correlated kinetic energy term: $\hat{\mathbf{T}}_{xy} = \frac{\hbar^2}{2m}(k_x^2+k_y^2+k_xk_y\sin\theta)$. The method can be extended to molecular surface scattering with arbitrary angles of incidence by applying a phase shift [68]. Additional correlation is possible by eliminating momentum values which are higher than an energy cutoff in Eq. (4.2) in the same spirit of eliminating grid points which are above a potential energy cutoff in coordinate space [59].

D. Computational Considerations

Summarizing the different approaches to grid construction, it should be emphasized that the purpose of the grid representation is to supply an effective algorithm for calculating the mapping induced by the Hamiltonian operator: $\phi = \mathbf{H}\psi$. The effectiveness of the algorithm can be judged by the operation count i.e by the number of floating point operations required to carry out the mapping. The most extreme case is when the Hamiltonian is represented as a full matrix. In this case the operation count scales as $O(N_g^2)$. For large multidimensional problems, this scaling relation becomes prohibitively expensive. This is in contrast to the mapping induced by the potential energy which in a grid coordinate representation is local and therefore scales linearly with N_g as $O(N_g)$. The bottle-neck of computation can be identified in the kinetic energy operation. At this point one should distinguish between one and multi-dimensional considerations.

In the general collocation representation, the kinetic energy operator Eq. (3.38) is a full matrix and therefore the mapping induced by it scales as $O(N_g^2)$. In the other extreme are the finite difference methods which are constructed from banded matrices and therefore scale linearly as $O(N_g)$. The linear scaling relation is at the expense of accuracy. In the Fourier method, due to the FFT algorithm, the scaling is semi-linear with N_g, $O(N_g \log N_g)$ with no price in accuracy. One can view the algorithm as an efficient means of performing the unitary transformation from coordinate to momentum space. An alternative to the FFT algorithm is to define directly the kinetic energy operator in coordinate space

$$\hat{\mathbf{T}}(\mathbf{x}) \quad = \quad \mathbf{Z^{-1}}\hat{\mathbf{T}}(\mathbf{k})\mathbf{Z} \; , \tag{4.3}$$

where $\mathbf{Z}_{jk} =< x_j|k >= 1/\sqrt{2\pi}e^{ikx_j}$ is the coordinate to momentum unitary transformation. The drawback to the use of equation (4.3) is that it is a full matrix operator scaling as $O(N_g^2)$. Since the FFT algorithm has an overhead of a factor of 3 to 5, there is a turnover appearing between $N_{g_{crit}} = 32$ to $N_{g_{crit}} = 96$ so that for $N_g < N_{g_{crit}}$ a direct transform becomes more efficient than the FFT algorithm. This finding is very sensitive to the particular computer architecture in use [59]. For example, very efficient FFT routines are available on vector and parallel computer architecture [69]. The superior scaling of the Fourier method has been the motivation for searching for other fast transforms to perform the kinetic energy operator [46]. Since in most of the present applications N_g is rather small, the usefulness of these transforms is marginal considering the added complications involved.

One of the recurring problems in using the Fourier method is the periodic boundary conditions. In some cases, such as scattering from a crystal surface, these boundary conditions match the physical problem. When a bound state problem is considered, the wavefunction at the boundary should be zero. Effectively such a condition is approximated by forcing the wavefunction at the boundary of the grid to be deep in the classical forbidden region. The amplitude of the wavefunction at the boundary can thus be made exponentially small.

Practically this means devoting some sampling points to the classically forbidden region. The extent of this region can be estimated from the semiclassical tunneling formula:

$$\psi(L) \quad \approx \quad e^{-\frac{1}{\hbar}\int_{l'}^{L} \sqrt{2\mu(V(x)-E)}dx} \tag{4.4}$$

where the buffer region extends from l to L with E as a typical energy. These boundary conditions fit the view of a wavepacket which becomes exponentially close to a band limited function with finite support. Absorbing boundary conditions are also extremely important [70–78]. Like the bound state boundary conditions they reduce to zero the amplitude of the wavefunction at the end of the grid.

Another related method to reduce the grid requirement is based on the superposition principle. The wavefunction and the propagation are split between two overlapping grids [79]. This method allows the separation of the asymptotic dynamics from the interaction part. Care must be taken that the transmission of amplitude from one grid to the other is gradual in space to avoid numerical problems of overflowing phase space by a sharp transmission function.

2. Multi-dimensional kinetic energy scaling

When a direct product multidimensional grid is constructed from D one dimensional grids: $N_g = N_1 \otimes N_2 \otimes N_3 \otimes ... N_D$. If the individual one-dimensional kinetic energy operation scales as $O(N_l^\alpha)$, then the total number of operations to calculate this term on all grid points becomes: $N_g/N_l O(N_l^\alpha) = N_g O(N_l^{\alpha-1})$. Since the total kinetic energy operator is the sum of kinetic energy operators on each degree of freedom, the total operation count will scale linearly with the total number of grid points $O(DN_g)$. These considerations still hold for the multidimensional skewed Fourier grid and for the adiabatically correlated grid [63]. The consequence is that high dimensional problems scale semi-linearly according to the number of grid points, with small dependence on the one-dimensional scaling of the kinetic energy operator. It then becomes more important to reduce the total number of grid points than to optimize the 1-D operation [60,63].

One of the methods to minimize the number of grid points is to use an adaptive grid, a grid which changes as the calculation progresses. For example, in a reactive scattering calculation for the initial state representation it is sufficient to include only the entrance channel. When the wavepacket evolves to sample more of the grid then the reactive channel is included. Adaptive grids are useful also in momentum space. Consider as an example a Coulomb explosion event or any sudden change from an attractive to a repulsive potential energy surface. As time proceeds the wavepacket accelerates and the momentum is shifted to higher values. Examining figure 4.7, it becomes clear that a grid that follows the wavefunction both in coordinate space and in momentum space will reduce the number of grid points by at least a factor of 15, which is the effective area ratio of the support of the wavepacket in phase space in relation to the total represented area required for the full dynamical encounter.

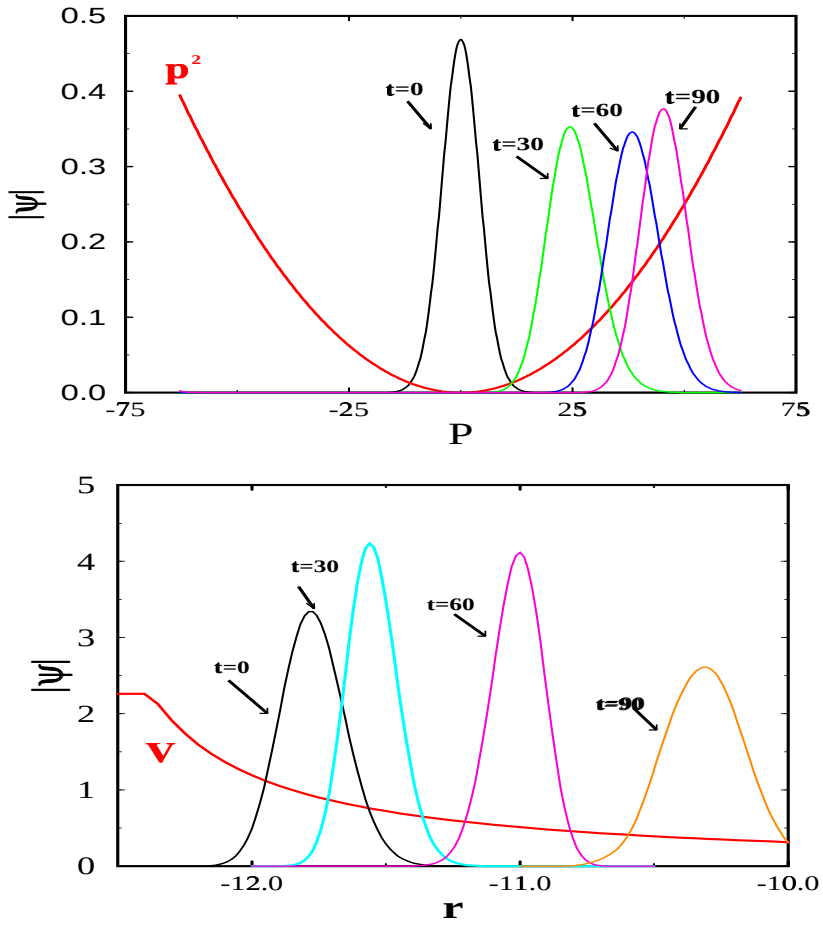

FIGURE 4.7 Wavepacket propagation in a Coulomb experiment simulation of the process $\mathbf{D}_2 \rightarrow 2\mathbf{D}^+$. Lower panel: absolute value of the wavefunction in position space superimposed on the repulsive Coulomb potential. The wavefunctions are labeled by the elapsed time from the ionization in atomic units. Upper panel: absolute value of the wavefunction in momentum space superimposed on the kinetic energy term P^2. Since the wavefunction is compact an adaptive grid which will follow the wavepacket in position and momentum space can reduce the number of grid points significantly.

Optimal positioning of the wavefunction becomes possible provided there is an interpolation scheme which allows a grid-to-grid transfer of the wavefunction. The collocation method in general and the Fourier method in particular are capable of extremely accurate and efficient interpolation aside from their intrinsic advantage in the representation of nonlocal operators. An extreme case of a continuously adaptive grid is provided in the interaction picture [80–85]. This representation continuously shifts the grid and therefore significantly reduces its size. The price paid is that the Hamiltonian of the problem becomes explicitly time dependent which complicates the propagation procedure.

V. PROPAGATION SCHEMES

The limelight now shifts to the time-energy phase space. A detailed description is beyond the scope of the present chapter has been recently reviewed [15]. The present focus will therefore be on the interrelations between the position-momentum phase space representation and the propagator representing operators in the time-energy phase space.

Propagation methods have in common the recursive application of an elementary mapping step which for the Hamiltonian operator, becomes:

$$\phi \quad = \quad \hat{\mathbf{H}}\psi \quad . \tag{5.1}$$

Since grid methods supply a very direct means to perform this mapping, the development of propagation schemes has been closely related to the development of grid methods. The propagation schemes supplement the elementary mapping by the additional operation of two

vectors $\phi_3 = \phi_1 + \phi_2$. This means that the propagator scheme becomes an effective agent to calculate recursively the mapping of a polynomial on an initial wavefunction:

$$\phi_N \quad = \quad \mathcal{P}_N(\hat{\mathbf{H}})\psi \quad , \tag{5.2}$$

where $\mathcal{P}_N$ is a polynomial of degree N. On this basis, propagation methods can approximate the mapping of any analytic function $f(z)$ of an operator under study on a wavefunction $\phi = f(\hat{\mathbf{H}})\psi$. With these concepts in mind, propagation techniques can be classified according to the function $f(z)$ which is approximated. For example, the evolution operator $\hat{\mathbf{U}}(t) = \exp(-i/\hbar\hat{\mathbf{H}}t)$ is represented by the function e^{-izt}. Table IV summarizes the classification according to the function $f(z)$. For more details see Ref. [15].

TABLE IV. Common functions in propagation schemes

	$f(z)$	use	reference
1	e^{-izt}	Evolution operator $\hat{\mathbf{U}}(t)$	[14,86]
	$\cos(zt)$, $\sin(zt)$		[87]
2	$e^{-z\tau}$	Relaxation, Diffusion	[88,89]
3	$e^{-(z-\alpha)^2\tau}$	Filtering	[90,91]
	$\int_0^T e^{-izt}g(t)dt$	Filter diagonalization	[92,93]
4	$\frac{i}{2\pi}\frac{1}{E-z}$	Raman spectra	[94]
	$\int_0^\infty e^{iEt}e^{-izt}dt$	Greens function	[95,96,60,97]
5	$\delta(z-E)$	Correlation functions	[98,99]
		Absorption spectra	[100]
	$\int_\infty^\infty e^{iEt}e^{-izt}dt$	Spectral density	[101]

Propagation schemes can also be classified by the type of polynomial used to carry out the approximation. Four families of polynomials have been used in conjunction with grid methods:

TABLE V. Classification of polynomials

	$\mathcal{P}_N$	Scheme	Recursion formula	Reference
1	Taylor		$\phi_n = \hat{\mathbf{H}}\phi_{n-1}$	[102]
	SOD		$\psi_{n+1} = \psi_{n-1} - i2\Delta t\hat{\mathbf{H}}\psi_n$	[8]
2	Chebychev	Spectral	$\phi_{n+1} = 2\hat{\mathbf{H}}\phi_n - \phi_{n-1}$	[14]
	Legendre		$(n+1)\phi_{n+1} = (2n+1)\hat{\mathbf{H}}\phi_n - n\phi_{n-1}$	[96]
3	Newton	Pseudo-spectral	$\phi_{n+1} = (\hat{\mathbf{H}} - x_n\hat{\mathbf{I}})\phi_n$	[103,15,97]
4	Lanczos	Krylov	$\hat{\mathbf{H}}\phi_n = \beta_{n-1}\phi_{n-1} + \alpha_n\phi_n + \beta_n\phi_{n+1}$	[104–107]
	Residum	$\phi_n = \hat{\mathbf{H}}^n\psi$		[108–110]

The diversity of these schemes means that when an effective grid representation is chosen a propagation scheme can be selected which will enable to calculate any observable of interest in a dynamical molecular encounter. This concludes the task of comparing simulation with experiment. In the next section, the relation of these propagation methods to a grid in the time-energy phase space will be investigated.

A. Time energy Grids

The description of the molecular encounter in the time-energy phase space is distinct from that in the position-momentum phase space. The first is an initial value problem while the latter is a boundary value problem. This distinction means that while in the position-momentum phase space the grid supplies a means of interpolation between the points. In contrast, in the time energy phase space the grid is used for extrapolation. The point is illustrated by comparing the second order differencing (SOD) time propagation scheme [8] to the finite difference (FD) scheme. The central differencing formula is used in both cases. In the second order FD method the derivatives are calculated at a point q_j by interpolating between the two neighbouring points; $\frac{\partial \psi_j}{\partial q} \approx \frac{\psi_{j+1}-\psi_{j-1}}{2\Delta q}$. In the SOD scheme the central differencing formula is used to extrapolate to a new point in time: $\psi_{n+1} \approx \psi_{n-1} + 2\Delta t \frac{\partial \psi}{\partial t}$.

The drawback of any extrapolation scheme in the time domain is that errors accumulate during the propagation. By changing the primary perspective to the energy domain an interpolation in the energy spectrum can replace the extrapolation, leading to superior convergence properties. Most of the high quality propagation schemes exploit this property. They use a spectral functional expansion in the energy variable to approximate the propagator. For example the Chebychev propagation scheme is a spectral expansion in the energy domain [15].

A representation in the energy variable can also be based on a grid construction. The Newtonian propagation methods [103,111,15] are based on such a concept. The primary interpolation grid is constructed in the energy eigenvalue domain. For example the grid points

can be chosen as the zeros of the Chebychev polynomial. This requires re-normalization of the Hamiltonian so that its eigenvalues will be contained in the interpolated region [15]. The grid points can also be extended into the complex plane in order to interpolate problems with complex eigenvalues [103,112,113].

Figure 5.1 shows an evolving wavepacket on the coordinate-time grid (q, t). Due to the slight unharmonicity of the potential used, the initially compact wavepacket disperses, which means that for long enough time the wavefunctions fills uniformly all the available coordinate space. Two methods of propagation are compared. In the left panels the propagation was carried out by interpolation (CH) in the energy domain while in the right panel by extrapolation (SOD). The upper panels represent the first two cycles of the oscillator wavefunction.

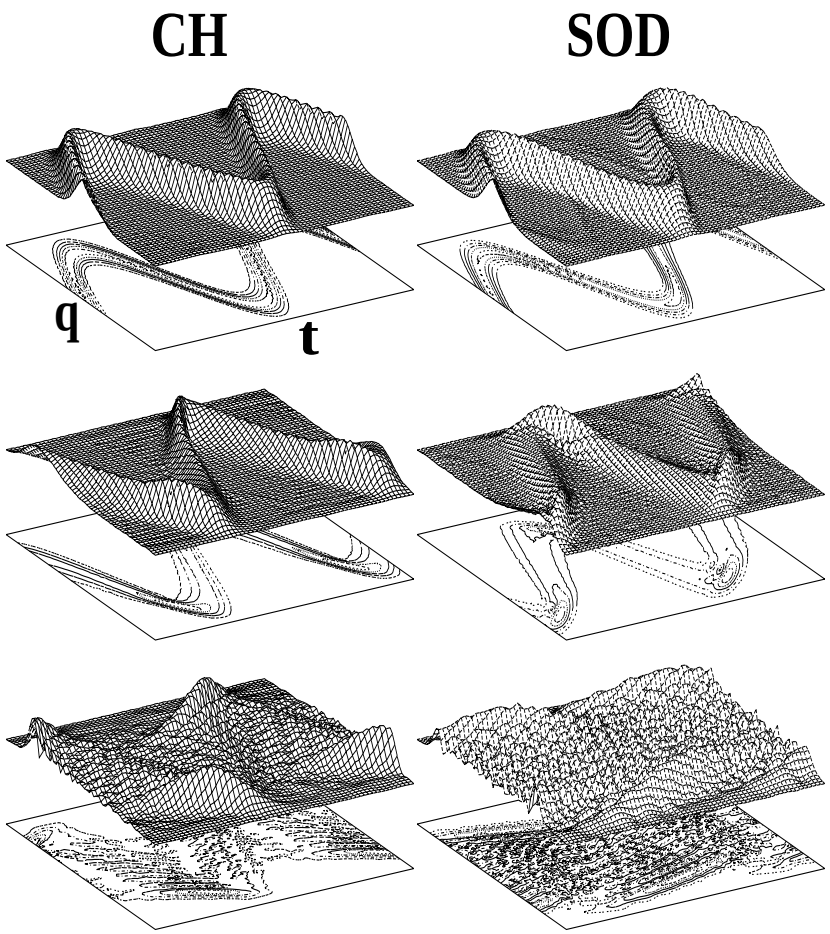

FIGURE 5.1 The evolution of an un-harmonic oscillator on a position-time grid (q, t). The

potential is $V(q) = q^2/2 - 2|q|/5$. Comparison between the evolution generated by the Chebychev (left) and SOD (right) propagation schemes. The interpolation grid consists of 32 Chebychev points with a time step $\Delta t = 0.05$. The propagation by the SOD scheme required the same numerical effort. The upper panel represents the first two cycles. The middle panels show the evolution after 10 cycles, and the lower panels shows the evolution after 50 cycles.

The first two cycles look quite similar although careful comparison shows that in the SOD scheme numerical dispersion appears already at this early stage. This can be seen as low amplitude signals between the waves. After approximately 10 cycles, further degradation appears in the SOD scheme: the phase of the main oscillation lags behind and the shape of the packet deteriorates. After approximately 50 cycles, the SOD scheme has lost the majority of the phase coherence. The interpolation scheme for the same conditions is converged to eight digits accuracy. It is important to point out that the SOD scheme preserves norm and energy to eight digits as well. This is an important observation common to many short time propagation schemes that the phase coherence is lost due to numerical dispersion much before the norm and energy show any significant error.

The number of grid points required to represent the time energy phase space directly determines the cost of the calculation. In the SOD scheme a stability analysis [94] determines the maximum time step as: $\Delta t_{max} \leq \hbar/|E_{max}|$ where $|E_{max}|$ is the largest eigenvalue of the Hamiltonian $\hat{\mathbf{H}}$ represented on the spatial grid. This inequality translates to the minimum number of grid points in the time-energy phase space $N_t > \Delta E \cdot t_s/2\hbar$ where ΔE is the range of eigenvalues of the Hamiltonian and t_s the total simulated time. The same minimum number of grid points in energy is found in a Chebychev based Newtonian energy grid $N_E > \Delta E \cdot t_s/2\hbar$. The methods differ completely in their convergence rate. Another difference is that in an energy interpolation scheme evaluation of the wavefunction at all the intermediate time steps is carried out simultaneously as well as backword propagation.

The above result, which is a consequence of the time-energy uncertainty principle, can be generalized to all propagation schemes. The size of the time step or the order of the interpolation polynomial is directly proportional to the volume of the time-energy phase

space. This observation reflects back to the grid construction in coordinate space. The energy range for optimal computational efficiency requires balancing and minimizing the energy range of each of the grid representations of the individual degrees of freedom.

B. Propagators for explicitly time dependent operators

In many physical applications the Hamiltonian is explicitly time dependent. The common solution for propagation in these explicitly time dependent problems is to use very small grid spacing in time, such that within each time step the Hamiltonian $\hat{\mathbf{H}}(t)$ is almost stationary. Under these semi-stationary conditions a short time propagation methods in the time energy phase space is employed. The drawback of this solution is that it is based on extrapolation, therefore the errors accumulate. Moreover, time ordering errors add with the usual numerical dispersion errors [108].

A global solution to the error accumulation problem is obtained by embedding the time-energy phase space of the system in a larger phase-space where interpolation in the energy domain becomes possible [111,114]. The first step is to add a grid in a new coordinate t'. The relation between the embedded wavefunction and the usual one subject to an initial state $\Psi(x,0)$ is defined as:

$$\Psi(x,t) \quad = \quad \int_{-\infty}^{\infty} dt' \; \delta(t'-t) \; \Phi(x,t',t) \tag{5.3}$$

where t' acts like an additional coordinate in the generalized Hilbert space [111] and $\Phi(x,t',t)$ is the solution of the time dependent Schrödinger equation represented by the (t,t') formalism,

$$i\hbar\frac{\partial}{\partial t}\Phi(x,t',t) \quad = \quad \mathcal{H}(x,t')\Phi(x,t',t) \qquad . \tag{5.4}$$

The $\mathcal{H}(x,t')$ operator is defined for a general time dependent Hamiltonian by,

$$\mathcal{H}(x,t') \quad = \quad H(x,t') - i\hbar\frac{\partial}{\partial t'} \qquad . \tag{5.5}$$

A simple proof has been derived by Peskin and Moiseyev [115]. Since $\mathcal{H}(x,t')$ is time (i.e t) independent, a time dependent solution of Eq (5.4) is given formally by,

$$\Phi(x,t',t) \;=\; \hat{U}(x,t',t)\Psi(x,t_0) \qquad \text{where} \qquad \hat{U}(x,t',t) \;=\; e^{-\frac{i}{\hbar}\mathcal{H}(x,t')t} \quad . \quad (5.6)$$

Equation (5.6) is solved by constructing a grid in the eigenspace domain of $\mathcal{H}$ [113], or by a spectral expansion in the energy domain [114]. Figure 5.2 shows such a solution for a system subject to a short pulse.

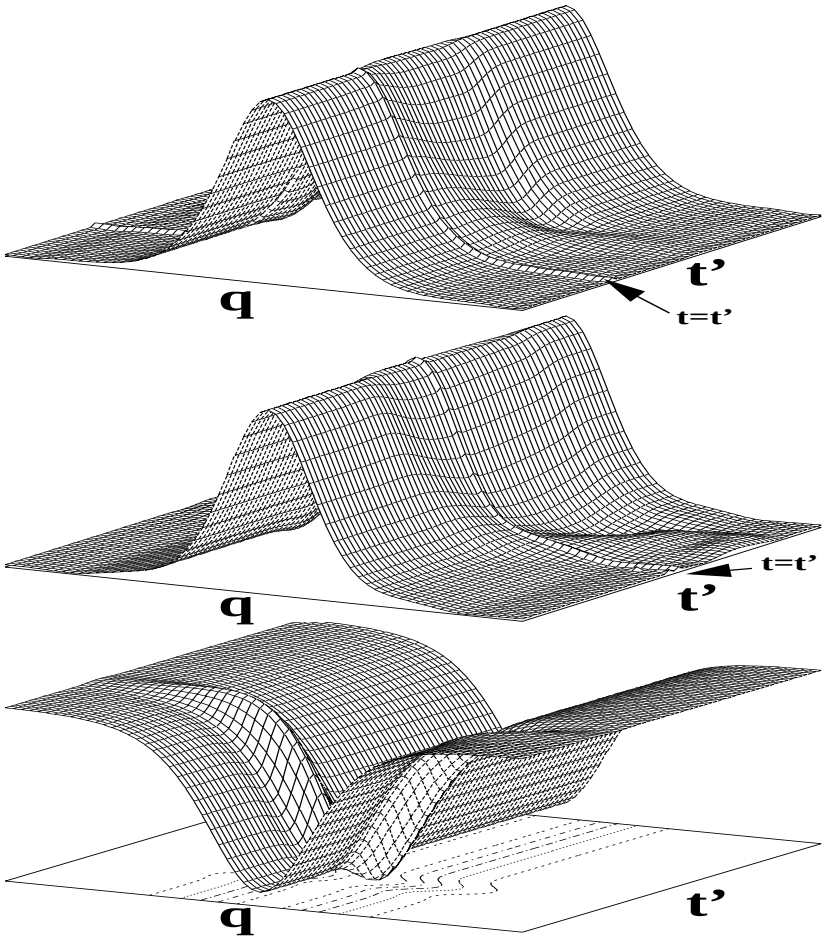

FIGURE 5.2 The wavefunction and the potential on an embedded representation q,t'. The lower panel displays the potential. In the q coordinate the potential has a well supporting bound states. In the t' direction the pulse appears as a hump in the potential at $t' = 24$. The upper panel shows the wavefunction at $t = 20$ just before the pulse. The arrow indicates the trace where $t = t'$ (enhanced in the figure). The wavefunction has not changed from its initial shape at $t = 0$ (a Gaussian wavefunction in q and a constant in t'). The middle panel displays the wavefunction immediately after the pulse at $t = 32$. The wavefunction

is excited. One should notice the flow of events from past to future.

The first derivative term $-i\hbar\frac{\partial}{\partial t}$ in equation (5.5) is responsible for a unidirectional propagation of events. An excitation located at time t' only influences the wavefunction after $t > t'$.

The hierarchy of grids required to represent faithfully an explicitly time dependent problem is as follows. A grid in the coordinate q to represent the $\{p, q\}$ phase space. A grid in the t' coordinate to represent the $\{E, t'\}$ phase space. And finally a grid in $\mathcal{E}$ allowing propagation in the $\{\mathcal{E}, t\}$ phase space.

VI. SUMMARY

Grid methods are at their best when they are used to represent wavepackets. Wavepackets are wavefunctions which posses a finite support in phase space. That is their amplitude outside a finite "volume" in phase-space becomes exponentially small when the supporting "volume" is increased. Pseudo-spectral representation methods for wavepackets are able to obtain exponential convergence of the calculation. This exponential convergence is a consequence of the dual representation strategy which is both pointwise on a grid as well as supported by a set of global functions. Within the pseudo-spectral family, the Fourier representation has particular importance since the grid and functional representation are symmetric. This symmetry enables the interpretation of the representation of the wavepacket on two grids, the position grid and on the momentum grid.

Since the wavepacket property is crucial in maintaining a high level of accuracy, during a simulation of a molecular encounter all measures should be employed to preserve this property. A counter example should stress the point. Coulombic wavefunctions are not wavepackets because of the singularity of the potential. For this reason pseudo-spectral methods loose much of their advantage. This accounts for the popularity of the semi-local FD and finite element grid methods for simulating encounters under the influence the Coulomb potential. For other applications the accuracy of the FD methods is not sufficient.

A phase-space picture is one of the most effective ways to study the representation qualities of a grid for a particular problem. The idea is to draw an energy confining boundary in phase-space. A wavefunction with an energy range within the restricting boundary, will decay exponentially in the classically forbidden regions, and is therefore classified as a wavepacket. Absorbing boundaries using imaginary potentials serve the same purpose of maintaining the wavepacket property for scattering encounters. It should therefore be designed in a such a way that the scattering wavefunction is maintained as a wavepacket on the grid at all stages of the propagation.

With these considerations in mind, the construction of an optimal simulation of a molecular encounter by grid methods, can be rationalized. The task begins by defining the global objective which is the observation under study. This objective determines the volume of time-energy phase-space i.e. the energy band and the time duration of the process. Once set, the energy band imposes a constraint on the position-momentum phase space description. In the representation of each individual degree of freedom, grid points or functional basis elements which have energy outside the predetermined energy band are eliminated. After this stage, global correlations should be imposed to eliminate composite points from the grid, both in the coordinate space and in "momentum" space, outside the energy band. In a particular application the sampling efficiency can be estimated by dividing the classically allowed regions of phase space by the phase-space volume of the grid.

Different optimal representation strategies can be employed for the individual degrees of freedom depending on the number of states contained in the energy band. If only a few states are present a spectral expansion in a basis is sufficient. An extreme example are the electronic degrees of freedom, which under normal conditions of molecular encounters one wavefunction is enough by the Born-Oppenheimer approximation and a few more can describe complicated nonadiabatic transitions. A spectral expansion is also common in the description of inelastic scattering of hydrogen from surfaces. For a higher density of states, pseudo-spectral grid representations become advantageous. These can be either DVR or Fourier based grids. The advantage of a fast transform such as the FFT is hardware dependent, typically when

$N_g > 50$. The duality between the pointwise base and the functional base in these methods means that the primary representation is a matter of convenience.

The representation on the spatial grid has strong influence on the volume of the time-energy phase-space. This is why a global approach to the simulation is required. The most effective methods of propagation are based on the use of the energy as the primary representation. This is because the propagator can be approximated as an interpolation as opposed to an extrapolation in the time domain.

Finally, the molecular dynamical simulation is only as good as the new insight it is able to supply. This task is beyond the scope of this chapter and depends mainly on human ingenuity.

ACKNOWLEDGMENTS

I wish to thank my colleagues, Dan Kosloff, Hillel Tal-Ezer, Charley Cerjan, David Tannor, Mark Ratner, Claude Leforestier, Rich Friesner, Nimrod Moiseyev, William Miller, Don Kouri, Stephan Gray, and Daniel Neuhauser for their contributions to this work, and to my students Roi Baer, Allon Bartana, Meli Naphcha, Eyal Fattal, Uri Psekin, Nir Ben-Tal, Rob Bisseling and Audrey Dell Hammerich. This research was supported by the Binational United States - Israel Science Foundation. The Fritz Haber Research Center is supported by the Minerva Gesellschaft für die Forschung, GmbH München, FRG.

REFERENCES

[1] E. J. Heller, J. Chem. Phys., **94**, 2723 (91).

[2] W. H. Miller, J. Chem. Phys., **95**, 9428 (1991).

[3] M. F. Herman and E. Kluk, Chem. Phys., **91**, 27 (1984).

[4] K. G. Kay, J. Chem. Phys., **100**, 2250 (1994).

[5] G. D. Billing, Inter. Rev. in Phys. Chem., **13**, 309 (1994).

[6] E. A. McCullough, R. E. Wyatt, J. Chem. Phys., **51**, 1253 (1969).

[7] E. A. McCullough, R. E. Wyatt, J. Chem. Phys., **54**, 3578 (1971).

[8] A. Askar and A. S. Cakmac, J. Chem. Phys., **68**, 2794 (1978).

[9] K. C. Kulander, K. J. Schafer, and J. L. Krause, In M. Gavrila, editor, *Atoms in Intense Radiation Fields*, number 1 in Advances in Atomic and Optical Physics, page 247, Academic, New York, (1992).

[10] M. D. Feit, J. A. Fleck Jr., and A. Steiger, J. Comp. Phys., **47**, 412 (1982).

[11] M. D. Feit and J. A. Fleck Jr., J. Chem. Phys., **78**, 301 (1983).

[12] D. Kosloff and R. Kosloff, J. Comp. Phys., **52**, 35 (1983).

[13] J.C. Light I.P. Hamilton and J.V. Lill, J. Chem. Phys., **82**, 1400 (1985).

[14] H. Tal-Ezer, R. Kosloff, J. Chem. Phys., **81**, 3967 (1984).

[15] R. Kosloff, Annu. Rev. Phys. Chem., **45**, 145 (1994).

[16] C. Lanczos, J. Math. Phys., **17**, 123 (1938).

[17] J.C. Light I.P. Hamilton, J. Chem. Phys., **84**, 306 (1986).

[18] R. A. Friesner, J. Chem. Phys., **85**, 1462 (1986).

[19] D. Gottlieb and S. A. Orszag, (SIAM, Philadelphia, 1977).

[20] M. Abramowitz and I. A. Stegun, *Handbook of Mathematical Functions*, (Dover, 1972).

[21] C. Schwartz, J. Math. Phys., **26**, 411 (1985).

[22] C. Lanczos, *Applied analysis*, (Prentice-Hall, Engelwood Cliffs, NJ, 1956).

[23] J. W. Cooley, and J. W. Tukey, Math. Comp., **19**, 297 (1965).

[24] H. J. Nussbaumer, *Fast Fourier Transform and Convolution Algorithms*, (Springer Verlag, Berlin, 2 edition, 1982).

[25] C. Temperton, J. Comp. Phys., **52**, 1 (1983).

[26] M. T. Heideman, D. H. Johnson, and C. S. Burrus, IEEE ASSP, **4**(1), 14 (1984).

[27] R. Kosloff, The Fourier Method, In C. Cerjan, editor, *Numerical Grid Methods and Their Application to Schrodinger's Equation*, page 175, Kluwer Academic Publishers, The Netherlands, (1993).

[28] G. G. Balint-Kurti, R. N. Dixon and Clay Marston, Grid methods for solving the Schrödinger equation and time dependent quantum dynamics of molecular photofragmentation and reactive scattering processes, Inter. Rev. in Phys. Chem., **11**, 317 (1992).

[29] E. T. Whittaker, Proc. Roy. Soc. Edinburgh, **35**, 181 (1915).

[30] H. Nyquist, Trans. AIEE 1, **47**, 617 (1928).

[31] C. E. Shannon, Proc. IRE (1949).

[32] C. Canuto, M. Y. Hussaini, A. Quarteroni and T. A. Zang, *Spectral methods in Fluid Dynamics*, (Springer, Berlin, 1987).

[33] A. Bacic and J. C. Light, J. Chem. Phys., **85**, 4594 (1986).

[34] A. Bacic and J. C. Light, J. Chem. Phys., **87**, 4008 (1987).

[35] G. C. Corey, J. W. Tromp and D. Lemoine, Fast Pesudospectral Algorithm in Curvilinear Coordinates, In C. Cerjan, editor, *Numerical Grid Methods and Their Application to Schrodinger's Equation*, page 1, Kluwer Academic Publishers, The Netherlands, (1993).

[36] J. C. Light, In J. Broeckhove and L. Lathouwers, editors, *Time Dependent Quantum Molecular Dynamics*, volume B 299, page 185, NATO ASI, (1992).

[37] D. E. Manolopolous and E. E. Wyatt, Chem. Phys. Lett., **152**, 23 (1988).

[38] D. E. Manolopoulos, Lobatto Shape Functions, In C. Cerjan, editor, *Numerical Grid Methods and Their Application to Schrodinger's Equation*, page 57, Kluwer Academic Publishers, The Netherlands, (1993).

[39] F. J. Lin and J. T. Muckerman, , Comp. Phys. Comm., **63**, 538 (1991).

[40] R. V. Weaver, J. T. Muckerman and T. Uzer, In J. Broeckhove and L. Lathouwers, editors, *Time Dependent Quantum Molecular Dyanmics*, volume B 299, page 381, NATO ASI, (1992).

[41] Y. Hoang, D. J. Kouri, and D. J. Hoffman, J. Chem. Phys., **101**, 10493 (1994).

[42] E. Fattal R. Baer and R. Kosloff, in preparation 1995.

[43] B. Jackson, J. Phys. Chem., **93**, 7699 (1989).

[44] F. Gygi, Phys. Rev. B, **48**, 11692 (1993).

[45] O. A. Sharfeddin, H. F. Bowen, D. J. Kouri and D. Hoffman, J. Comp. Phys., **100**, 294 (1992).

[46] R. H. Bisseling and R. Kosloff, J. Comp. Phys., **59**, 136 (1985).

[47] D. Lemoine, J. Chem. Phys., **101**, 4350 (1994).

[48] A. E. Siegman, Optics Lett., **1**, 13 (1977).

[49] J. D. Talman, J. Comp. Phys., **29**, 35 (1978).

[50] J. D. Talman, Comp. Phys. Comm., **30**, 93 (1983).

[51] R. N. Bracewell, *The Fourier Transform and its Applications*, (Mc Graw-Hill, New York, 1978).

[52] A. Besprozvannaya and D. Tannor, Comp. Phys. Comm., **63**, 569 (1991).

[53] Y. Shi and D. Tannor, J. Chem. Phys., **92**, 2517 (1990).

[54] R. C. Mowrey, H. F. Bowen and D. J. Kouri, J. Chem. Phys., **86**, 2441 (1987).

[55] R. C. Mowrey and D. J. Kouri, J. Chem. Phys., **86**, 6140 (1987).

[56] R. C. Mowrey, Y. Sun and D. J. Kouri, J. Chem. Phys., **91**, 6519 (1989).

[57] G. D. Billing, The Dynamics of Molecule-Surface Interaction, Comp. Phys. Rep., **12**, 383 (1990).

[58] G. R. Darling and S. Holloway, J. Chem. Phys., **101**, 3268 (1994).

[59] M.-N. Carre and D. Lemoine, J. Chem. Phys., **101**, 5305 (1994).

[60] D. T. Colbert and W. H. Miller, J. Chem. Phys., **96**, 1982 (1992).

[61] O. A. Shrafeddin and J. C. Light, J. Chem. Phys., **102**, 3622 (1995).

[62] G. C. Corey and D. Lemoine, J. Chem. Phys., **97**, 4115 (1992).

[63] R. A. Friesner, J. A. Bentley, M. Menou and C. Leforestier, J. Chem. Phys., **99**, 324 (1993).

[64] C. Leforestier and R. Friesner, An Adiabatic Pseudo-Spectral Representation of Multidimensional Molecular Potentials, In C. Cerjan, editor, *Numerical Grid Methods and Their Application to Schrodinger's Equation*, page 69, Kluwer Academic Publishers, The Netherlands, (1993).

[65] J. Antikainen, R. A. Friesner and C. Leforestier, J. Chem. Phys., **102**, 1270 (1995).

[66] D. P. Peterson and D. Midelton, Informat. Contr., **5**, 279 (1962).

[67] R. H. Bisseling and R. Kosloff, J. Comp. Phys., **76**, 243 (1988).

[68] G. J. Kroes and R. C. Mowrey, J. Chem. Phys., **101**, 805 (1994).

[69] P. N. Swarztrauber, *Parallel Computation*, (Academic Press, New York, 1982).

[70] C. Leforestier and R. E. Wyatt, Chem. Phys. Lett., **78**, 2334 (1983).

[71] R. Kosloff and D. Kosloff, J. Comp. Phys., **63**, 363 (1986).

[72] , D. Neuhauser and M Baer, J. Chem. Phys., **90**, 4351 (1989).

[73] M. S. Child, Mol. Phys., **72**, 89 (1991).

[74] A. Vibok and G.G. Balint-Kurti, J. Chem. Phys., **96**, 7615 (1992).

[75] G.G. Balint-Kurti and A.Vibok A, Complex Absorbing Potentials in Time Dependent Quantum Dynamics, In C. Cerjan, editor, *Numerical Grid Methods and Their Application to Schrodinger's Equation*, page 412, Kluwer Academic Publishers, The Netherlands, (1993).

[76] C. W. MacCurdy, C. K. Stround, , Comp. Phys. Comm., **63**, 323 (1991).

[77] T. Seideman and W. H. Miller, J. Chem. Phys., **97**, 2499 (1992).

[78] D. Acias, S. Brouard and J. G. Muga, Chem. Phys. Lett., **228**, 672 (1995).

[79] R. Heather and H. Metiu, J. Chem. Phys., **86**, 5009 (1987).

[80] J. Zang, , Chem. Phys. Lett., **160**, 417 (1989).

[81] J. Zang, , J. Chem. Phys., **92**, 324 (1990).

[82] J. Zang, Comp. Phys. Comm., **63**, 28 (1991).

[83] C. J. Williams, J. Qian and D. J. Tannor, J. Chem. Phys., **95**, 1721 (1991).

[84] D. J. Tannor A. Besprozvannaya and C. J. Williams, J. Chem. Phys., **96**, 2998 (1992).

[85] J. Kugar and D. H. Meyer, J. Chem. Phys., **90**, 566 (1989).

[86] T. J. Park and J. C. Light, J. Chem. Phys., **85**, 5870 (1986).

[87] S. K. Gray, , J. Chem. Phys., **96**, 6543 (1992).

[88] R. Kosloff and H. Tal-Ezer, Chem. Phys. Lett., **127**, 223 (1986).

[89] N. Agmon and R. Kosloff, J. Phys. Chem., **91**, 1988 (1987).

[90] A. D. Hammerich, J. G. Muga and R. Kosloff, Isr. J. Chem., **29**, 461 (1989).

[91] Y. Zeiri, E. Fattal and R. Kosloff, J. Chem. Phys., **102**, 1859 (1995).

[92] D. Neuhauser, J. Chem. Phys., **93**, 2611 (1990).

[93] D. Neuhauser, J. Chem. Phys., **100**, 5076 (1994).

[94] R. Kosloff, J. Phys. Chem., **92**, 2087 (1988).

[95] W. Zhu, Y. Hoang, D. J. Kouri, M. Arnold and D. J. Hoffman, Phys. Rev. Lett., **72**, 1310 (1994).

[96] D. J. Kouri, W. Zhu, Y. Hoang, and D. J. Hoffman, Chem. Phys. Lett., **220**, 312 (1994).

[97] S. Aurbach and C. Leforestier, Comp. Phys. Comm., **78**, 55 (1994).

[98] R. Baer and R. Kosloff, Chem. Phys. Lett., **200**, 183 (1992).

[99] R. Baer and R. Kosloff, J. Phys. Chem., **99**, 2534 (1995).

[100] Bernt Hartke, Ronnie Kosloff and Sanford Ruhman, Chem. Phys. Lett., **158**, 238 (1989).

[101] W. Zhu, Y. Huang, D. J. Kouri, C. Chandler and D. J. Hoffman, Chem. Phys. Lett., **217**, 73 (1994).

[102] Y. Sun, D. J. Kouri, D. W. Schwenke and D. G.Truhlar, Comp. Phys. Comm., **63**, 51 (1991).

[103] M. Berman, R. Kosloff and H. Tal-Ezer, J. Phys. A, **25**, 1283 (1992).

[104] G. Moro and J. H. Freed, , J. Chem. Phys., **74**, 3757 (1981).

[105] H. Köpel, L. S. Cederbaum, W. Domcke, J. Chem. Phys., **77**, 2014 (1982).

[106] A. Nauts and R. E. Wyatt, Phys. Rev. Lett., **51**, 2238 (1983).

[107] R. E. Wyatt, , Adv. Chem. Phys., **73**, 231 (1989).

[108] H. Tal Ezer, R. Kosloff, and C. Cerjan, J. Comp. Phys., **100**, 179 (1992).

[109] C. Leforestier, R. Bisseling, C. Cerjan, M. Feit, R. Friesner, A. Guldberg, A. D. Hammerich, G. Julicard, W. Karrlein, H. Dieter Meyer, N. Lipkin, O. Roncero and R. Kosloff, J. Comp. Phys., **94**, 59 (1991).

[110] C. Cerjan and R. Kosloff, Phys. Rev. A, **47**, 1842 (1993).

[111] U. Peskin, R. Kosloff, and N. Moiseyev, J. Chem. Phys., **100**, 8849 (1994).

[112] A. Bartana, R. Kosloff and D. J. Tannor, J. Chem. Phys., **99**, 196 (1993).

[113] U. Banin, A. Bartana, S. Ruhman and R. Kosloff, J. Chem. Phys., **101**, 8461 (1994).

[114] G. Yao and R. E. Wyatt, J. Chem. Phys., **101**, 1904 (1994).

[115] U. Peskin and N. Moiseyev, J. Chem. Phys., **99**, 4590 (1993).